https://doi.org/10.5194/egusphere-2026-5549
Preprint. Discussion started: 22 September 2026

A novel approach for efficient rain enhancement through the combined glaciogenic and hygroscopic cloud seeding

Weixi Shu[1], Danhong Fu[2,3], Xueliang Guo[2], Ling Yang[1], Xiaolu Liu[4]

[1]Department of Electronic Engineering and Institute of Low-Altitude Meteorological Intelligence Technology, Chengdu University of Information Technology (CUIT), Chengdu, 610225, China
[2]Laboratory of Cloud-Precipitation Physics and Severe Storms (LACS), Institute of Atmospheric Physics, Chinese Academy of Sciences (CAS), Beijing, 100029, China
[3]School of Earth and Planetary Sciences, University of Chinese Academy of Sciences (UCAS), Beijing, 100049, China
[4]Weather Modification Center of Sichuan Province, Chengdu, 610072, China

Correspondence to: Danhong Fu (fudanhong@mail.iap.ac.cn); Xueliang Guo (guoxl@mail.iap.ac.cn)

Abstract. Rain enhancement by artificial cloud seeding is widely used to increase water resource in arid and semi-arid regions of the world. However, large uncertainties in terms of cloud seeding and its effectiveness remain. This study proposes a novel approach for efficient rain enhancement of convective clouds with warm cloud base by combining glaciogenic seeding with silver iodide (AgI) and hygroscopic seeding with cloud condensational nuclei (CCN). The numerical simulation experiments through the WRF (Weather Research and Forecasting) model are systematically conducted and indicate that comparing to the control (unseeded) experiment, the combination of an earlier hygroscopic CCN seeding in the low warm layers at a seeding rate of 10^{13} s^{-1} and the subsequent glaciogenic AgI seeding in the upper mixed-phase layers at a seeding rate of 0.09 g s^{-1} can increase the surface rainfall up to 57%, which is seven times higher than 7.97% in a single glaciogenic seeding and nearly three times higher than 20.74% in a single hygroscopic seeding, showing a much stronger rain enhancement rate in the new approach. It is found that the earlier hygroscopic seeding in warm cloud layers is able to greatly enhance the supercooled liquid water (SLW) content in cold cloud layers through updraft lifting and create a much more advantageous condition suitable for the subsequent glaciogenic cloud seeding. Moreover, the combined cloud seeding approach also causes much stronger dynamic effect than any individual cloud seeding approach, and significantly enhances precipitation efficiency of convective clouds with warm cloud base. The novel cloud seeding approach has potential application in rain enhancement operation in middle and high latitudes in the world.

1 Introduction

Cloud seeding aims at enhancing precipitation of clouds, since cloud precipitation efficiency, defined as the ratio of the amount rain reaching the ground to the amount of water vapor entering the cloud base, is often less than unity (Fankhauser et al., 1988; Gao and Li, 2011). Atmospheric water budget reveals that only approximately 11% of the moisture converging into a convective cloud ultimately reaches the surface as precipitation (Braham, 1952). Therefore, despite many scientific

https://doi.org/10.5194/egusphere-2026-5549
Preprint. Discussion started: 22 September 2026

uncertainties in cloud seeding, it has been widely used to enhance precipitation in many arid and semi-arid regions in the world.

There are two principal cloud seeding techniques. One is so-called glaciogenic cloud seeding, which is to disperse efficient ice nuclei, such as silver iodide (AgI) particles, solid or liquid carbon dioxide into the supercooled mixed-phase clouds, and causes heterogeneous or homogenous glaciation of the supercooled liquid water (SLW), leading to the formation of precipitation (Geerts and Rauber, 2022). The other is hygroscopic cloud seeding, which is to disperse large salt particles near cloud base, and accelerates collision-coalescence warm rain process, enhancing the surface precipitation (National Research Council, 2003). Both glaciogenic cloud seeding and hygroscopic cloud seeding have been widely used in weather modification community in the world (Bruintjes et al., 1999; National Research Council, 2003; Silverman, 2003; Garstang et al., 2005; Rosenfeld et al., 2010; Guo et al., 2015; Freud et al., 2015; French et al., 2018; Flossmann et al., 2019; Tessendorf et al., 2021; Prabhakaran et al., 2023).

It is the most challenging work to separate artificial seeding effect from large natural variability in cloud seeding (Pokharel et al., 2014; Guo et al., 2015; Wang et al., 2019). Numerical models incorporating with cloud seeding process are often used to explain physical mechanisms of cloud seeding (Orville, 1996; Garstang et al., 2005). For glaciogenic seeding, the early studies used cloud models incorporating AgI nucleation processes derived from cloud chambers (Blair et al., 1973; DeMott, 1995), to investigate the effects of AgI seeding on clouds and precipitation (Meyers et al., 1995; Guo et al., 2006, 2007). With developing cloud-resolving mesoscale models such as the Weather Research and Forecasting (WRF) model, AgI nucleation process was also incorporated into cloud microphysics schemes in mesoscale models to investigate the effects of AgI seeding on clouds and precipitation (Fang et al., 2009; Xue et al., 2013a, b; He et al., 2023). The cloud-resolving mesoscale models with cloud seeding process have also been used for forecasting and simulating seeding condition and evaluating seeding effectiveness in operational weather modification activities in China (Lou et al., 2012; He et al., 2023; Wei et al., 2024), the United States (Mazzetti et al., 2023), Australia (Chen et al., 2023), and the United Arab Emirates (Fonseca et al., 2022). These studies have demonstrated that the AgI seeding in convective regions with a high SLW can increase ice crystal concentrations through deposition and freezing nucleation, promoting rapid growth of ice-phase hydrometeors (Xue et al., 2016; Omanovic et al., 2024; Dong et al., 2026), which ultimately enhances surface precipitation upon the melting of large ice particles (French et al., 2018). Meanwhile, the seeding-induced additional latent heat release from deposition and freezing can trigger significant interactions between cloud microphysics and dynamics, invigorating updrafts and prolonging cloud lifetime, and causing more precipitation (Orville and Chen, 1982; Guo et al., 2015; Flossmann et al., 2019).

For hygroscopic seeding, substantial progresses have been achieved in simulating hygroscopic cloud condensational nuclei (CCN) seeding effects on warm-rain processes (Cooper et al., 1997; Caro et al., 2002; Tessendorf et al., 2021). By explicitly introducing appropriately sized CCN distributions into spectral bin or double-moment cloud microphysics schemes, previous studies have shown that an optimal concentration of hygroscopic particles released into the warm-cloud region can broaden the cloud droplet size distribution through water vapor competition, accelerating warm rain processes of droplet autoconversion and collision-coalescence, thereby enhancing warm-rain efficiency (Yin et al., 2000; Segal et al., 2004; Lin et al., 2023). It was found that ultra-giant CCN with diameters greater than 10 μm, such as salt powder can serve directly as raindrop embryos to promote raindrop formation (Jensen and Lee, 2008; Hoffmann and Feingold, 2021).

Generally, glaciogenic cloud seeding is often used for rain enhancement of clouds in which mixed-phase and ice microphysics are dominant, while hygroscopic cloud seeding is used for rain enhancement of convective clouds with dominant warm rain process (Kuba and Murakami, 2010; Chen et al., 2025). However, both warm and cold rain processes are equally important in massive convective clouds with warm cloud base, especially for convective clouds in warm seasons (Sun et al., 2016; Beydoun et al., 2023). Moreover, warm and cold regimes are not physically independent in natural mixed-phase convective clouds, and they interact through complex exchanges of mass, momentum and heat (Andreae et al., 2004; Rosenfeld et al., 2008; Shu et al., 2022), in particular, the low-level warm liquid water can directly regulate SLW through transporting into the upper mixed-phase regime (Lee et al., 2016; Tonttila et al., 2022), leading to a delayed but intensified cold-rain precipitation and thereby increasing cold-cloud precipitation efficiency (Cui et al., 2011; Fan et al., 2018; Tonttila et al., 2021), while abundant SLW is a crucial prerequisite for effective AgI glaciogenic seeding and the associated latent-heating feedbacks (DeMott, 1995; Rauber et al., 2019).

Inspired by previous results about strong interactions between warm and cold cloud microphysics in convective clouds and low-efficiency limitations for current individual cloud seeding, this study aims to proposal a novel approach for more efficient cloud seeding by combining both hygroscopic and glaciogenic cloud seeding. Hence, systematic and thorough numerical simulation experiments are designed and conduced to quantitively compare the combined cloud seeding with individual cloud seeding for convective clouds with warm cloud base. The associated mechanisms in terms of cloud microphysics and dynamics are elucidated.

The paper is organized as follows. Section 2 is methodology to describe the model and its configuration, seeding parametrizations and data used in this study. Section 3 introduces the study case and the setup of seeding experiments. Section 4 presents the effects of different cloud seeding on clouds and precipitation and the associated mechanisms. Section 5 is conclusions and discussion.

2 Methodology

2.1 The model and configuration

An idealized 3D framework in the WRF model incorporating with both glaciogenic and hygroscopic seeding schemes is employed in this study in order to simplify complex and nonlinear interactions among atmospheric, orographic and boundary processes. The numerical simulations are initialized with a horizontal homogenous sounding extracted from a real-case WRF simulation. The real-case simulation is configured with three two-way nested domains centered at (29.5°N, 103.5°E). The horizontal grid spacings are 12, 4, and 1.333 km, with corresponding grid points of 437×354, 505×460, and 547×511,

https://doi.org/10.5194/egusphere-2026-5549
Preprint. Discussion started: 22 September 2026

respectively. The vertical grid consists of 46 terrain-following levels with the model top set at 50 hPa. The integration time steps are 72, 24, and 8 s, respectively, for the three domains.

The convection in the idealized model is initiated by a thermal bubble with a maximum temperature perturbation of 3 K centered at a height of 1.5 km. The bubble has a horizontal radius of 10 km and a vertical radius of 1.5 km, and the perturbation temperature decreases toward the bubble edge following a cosine squared function. The idealized domain features a horizontal grid spacing of 1 km with 400×400 grid points, which is sufficient to resolve the primary features of the convective clouds. The model uses 47 vertical layers and is integrated with a time step of 6 s. Model outputs are archived every 10 min to facilitate a comprehensive analysis of convective evolution and seeding responses. Consistent with the typical distribution characteristics of continental aerosols (Weston et al., 2022), the near-surface background aerosol concentration in the model is set to be 300 cm^{-3}, decaying exponentially with height.

2.2 Glaciogenic and hygroscopic cloud seeding schemes

Glaciogenic cloud seeding scheme is implemented in the Thompson microphysics scheme in WRF v4.2 model (Skamarock et al., 2019) through incorporating with the silver iodide (AgI) cloud-seeding parameterization scheme (Guo et al., 2006, 2007). The scheme includes AgI-induced heterogeneous ice nucleation through contact freezing and deposition nucleation. Contact freezing occurs when AgI particles are collected by supercooled cloud droplets and raindrops through Brownian motion and inertial impaction, whereas deposition nucleation occurs under saturation with respect to ice, and AgI activation depends on the degree of supercooling.

Hygroscopic cloud seeding is also implemented in the Thompson microphysics scheme of WRF model. The hygroscopic behavior of seeded CCN is represented through a prescribed hygroscopicity parameter κ, rather than through explicit treatment of individual chemical species. The size distribution of the unactivated seeded CCNs is assumed to follow a lognormal distribution,

$$n_r = \frac{n_h}{r\sqrt{2\pi}\ln\sigma_g}\exp\left\{\frac{-[\ln(r/r_g)]^2}{2(\ln\sigma_g)^2}\right\}, \quad (1)$$

where r is the CCN radius, n_r is the number concentration of seeded CCNs within a given radius interval, and n_h is the total number concentration of the seeded CCNs. σ_g is the geometric standard deviation, and r_g is the median radius. In this study, the size distribution parameters are assumed to be constant at $\sigma_g = 1.8$ and $r_g = 0.04\,\mu m$, which defines the CCN size distribution used in the activation calculation.

The activation of seeded hygroscopic CCN particles into cloud droplets is treated using the CCN activation framework of Thompson and Eidhammer (2014), which is based on Köhler theory (Köhler, 1936) and the parcel-model calculations of Feingold and Heymsfield (1992). At each model grid point and time step, the fraction of available CCN activated into cloud droplets is determined from a five-dimensional lookup table as

$$n_{act} = f_{act}(T, w, n_h, r_g, \kappa)n_h, \quad (2)$$

https://doi.org/10.5194/egusphere-2026-5549
Preprint. Discussion started: 22 September 2026

where f_{act} is the fraction of available CCN activated into cloud droplets. The lookup table is constructed as a function of CCN number concentration n_h, vertical velocity w, temperature T, CCNs mean radius r_g, and hygroscopicity parameter κ following Thompson and Eidhammer (2014). During the simulation, T, w, and n_h are obtained from the model state. For a given temperature level, the activation fraction is calculated by bilinear interpolation in logarithmic n_h–w space according to

$$f_{act} = (1-\alpha)(1-\beta)f_{i-1,j-1} + \alpha(1-\beta)f_{i,j-1} + \alpha\beta f_{i,j} + (1-\alpha)\beta f_{i-1,j} \,, \tag{3}$$

where

$$\alpha = \frac{ln n_h - ln n_{i-1}}{ln n_i - ln n_{i-1}} \,, \tag{4}$$

$$\beta = \frac{ln w - ln w_{j-1}}{ln w_j - ln w_{j-1}} \,, \tag{5}$$

Here, n_{i-1} and n_i are the two tabulated CCN concentrations surrounding the model-predicted n_h, while w_{j-1} and w_j are the corresponding tabulated vertical velocities surrounding the model-predicted w. The quantities $f_{i-1,j-1}$, $f_{i,j-1}$, $f_{i,j}$, and $f_{i-1,j}$ are the activation fractions at the four surrounding lookup-table points. The model temperature is mapped to the nearest tabulated temperature level, with temperature levels separated by 10 K, rather than being interpolated between adjacent temperature levels. The CCNs mean radius r_g and hygroscopicity parameter κ are fixed at 0.04 μm and 0.4, respectively.

For every newly activated cloud droplet, one CCN particle is removed from the n_h population. The newly activated droplet is assigned an initial diameter of 4 μm for the calculation of condensational growth.

The local tendency of the number mixing ratio of seeded hygroscopic CCN (N_h) in the model is determined by both 3D dynamic advection and microphysical source/sink terms. The tendency equation for N_h can be expressed as,

$$\frac{\partial N_h}{\partial t} = D_{N_h} + S_{seed} - S_{scav} - S_{act} - S_{hom} + P_{evap} \tag{6}$$

where $N_h = n_h/\rho$ and ρ is air density; D_{N_h} denotes resolved 3D advection term. The term S_{seed} represents the source of seeded CCN particles released into the model. In this study, the prescribed CCN seeding rate ranges from 10^9 to 10^{16} s^{-1} in the hygroscopic and combined seeding experiments.

The scavenging sink S_{scav} represents the collection of CCN particles by rain, snow, and graupel and is written as

$$S_{scav} = S_r + S_s + S_g \,, \tag{7}$$

The individual scavenging rates are calculated as

$$S_r = \frac{1}{\rho} F_\rho \frac{\pi}{4} a_r \Gamma(\mu_r + b_r + 3) E_{ra}\, n_h N_{0r} (\lambda_r + f_r)^{-(\mu_r + b_r + 3)} \,, \tag{8}$$

$$S_s = \frac{1}{\rho} F_\rho \frac{\pi}{4} a_s E_{sa}\, n_h M_{b_s+2}^{(s)} \,, \tag{9}$$

$$S_g = \frac{1}{\rho} F_\rho \frac{\pi}{4} a_g \Gamma\left(\mu_g + b_g + 3\right) E_{ga}\, n_h N_{0g} \lambda_g^{-(\mu_g + b_g + 3)} \,, \tag{10}$$

where ρ is air density $F_\rho = (\rho_0/\rho)^{1/2}$ is the air density correction factor. The coefficients a_x and b_x (x = r, s, g) are the empirical parameters in the terminal-velocity relations for rain, snow, and graupel, respectively. μ_r and μ_g are the shape parameters of the rain and graupel size distributions, and Γ denotes the gamma function. E_{ra}, E_{sa}, and E_{ga} are the CCNs collection

https://doi.org/10.5194/egusphere-2026-5549
Preprint. Discussion started: 22 September 2026

efficiencies for rain, snow, and graupel, respectively, accounting for Brownian diffusion, interception, and inertial impaction following Wang et al. (2010); N_{0r} and N_{0g} are the corresponding intercept parameters; λ_r and λ_g are the slope parameters; f_r is the exponential correction parameter in the rain terminal-velocity relation; and $M_{b_s+2}^{(s)}$ is the corresponding moment of the snow particle size distribution (Thompson et al., 2008).

S_{act} denotes the depletion of hygroscopic CCNs due to activation into cloud droplets. S_{hom} denotes the depletion of deliquesced hygroscopic CCNs through homogeneous ice nucleation under sufficiently cold and ice-supersaturated conditions (T<238 K and ice supersaturation ≥0.4), following Koop et al. (2000). The source term P_{evap} represents the regeneration rate of CCNs back into the atmosphere due to evaporation is written as

$$P_{evap} = P_{evap,c} + P_{evap,r} \ , \qquad (11)$$

where $P_{evap,c}$and $P_{evap,r}$ denote CCNs regeneration associated with the complete evaporation of cloud droplets and raindrops, respectively, with one CCN returned to the available CCN population for each completely evaporated hydrometeor (Thompson and Eidhammer, 2014).

After activation, cloud droplets are treated by the bulk microphysics scheme and subsequently evolve through condensation, collision–coalescence, autoconversion, accretion, freezing, and other hydrometeor conversion processes.

2.3 The data

The initial and lateral boundary conditions for the mesoscale numerical simulations were derived from the fifth generation European Centre for Medium-Range Weather Forecasts (ECMWF) atmospheric reanalysis (ERA5; https://www.ecmwf.int/). This reanalysis fields have a horizontal resolution of 0.25°×0.25° and a temporal interval of 3 h, covering the period from 2100 UTC 5 August to 0000 UTC 7 August 2025. Surface precipitation observations over the southwest China were obtained from the automatic weather station network maintained by the National Meteorological Data Center of China Meteorological Administration (CMA; https://data.cma.cn/). Radar observations were collected by the S-band Doppler weather radar located in Chengdu, Sichuan Province (30.41 °N, 104.23 °E; elevation: 107 m). The radar has a beamwidth of around 1°, a range resolution of 250 m on each beam, and operates in a volume coverage pattern with nine elevations angles (0.58, 1.58, 2.48, 3.48, 4.38, 6.08, 9.98, 14.68, and 19.58) every 6 min.

3 The study case and setup of seeding experiments

3.1 The study case

A convective precipitation event occurred on 6 August 2025 in central Sichuan Province, southwestern China, is selected to investigate the combined seeding effects. Abundant moisture transport, strong convective instability, and complex terrain provide suitable conditions for the initiation and development of convective clouds over the Sichuan basin (Qian et al., 2015; Xia et al., 2021), and convection often exhibit a deep mixed-phase cloud in warm seasons (Huang and Cui, 2015; Qi et al.,

https://doi.org/10.5194/egusphere-2026-5549
Preprint. Discussion started: 22 September 2026

2022). At 0000 UTC, synoptic pattern at 200 hPa was characterized by an anticyclonic circulation over southwestern China (Fig. 1a). The pronounced upper-level divergence associated with the anticyclone center provided favorable dynamical support for ascent in the middle and lower troposphere. To the north of the anticyclone, a region of dense streamlines indicated the upper-level jet stream, which dynamically sustained the anticyclonic structure. By 0600 UTC, the anticyclonic circulation had slightly intensified, further facilitating the maintenance and development of the convective over the Sichuan Basin (Fig. 1b).

At 600 hPa, a low-pressure system was located over southern Sichuan at 0000 UTC. The prevailing airflow on the northern flank of this system transported abundant moisture from the southeastern maritime regions into the Sichuan Basin, providing a favorable moisture supply for cloud development and precipitation (Fig. 1c). Simultaneously, the low- and mid-level airflow interacted with the complex terrain of western Sichuan. The resulting orographic lifting, together with the upper-level divergence at 200 hPa, established an environment favorable for convective initiation and development. By 0600 UTC, the moisture transport into the Sichuan Basin strengthened markedly, with water vapor flux exceeding 8 g s^{-1} hPa^{-1} cm^{-1}, which further supported the intensification and persistence of the convective event (Fig. 1d).

https://doi.org/10.5194/egusphere-2026-5549
Preprint. Discussion started: 22 September 2026

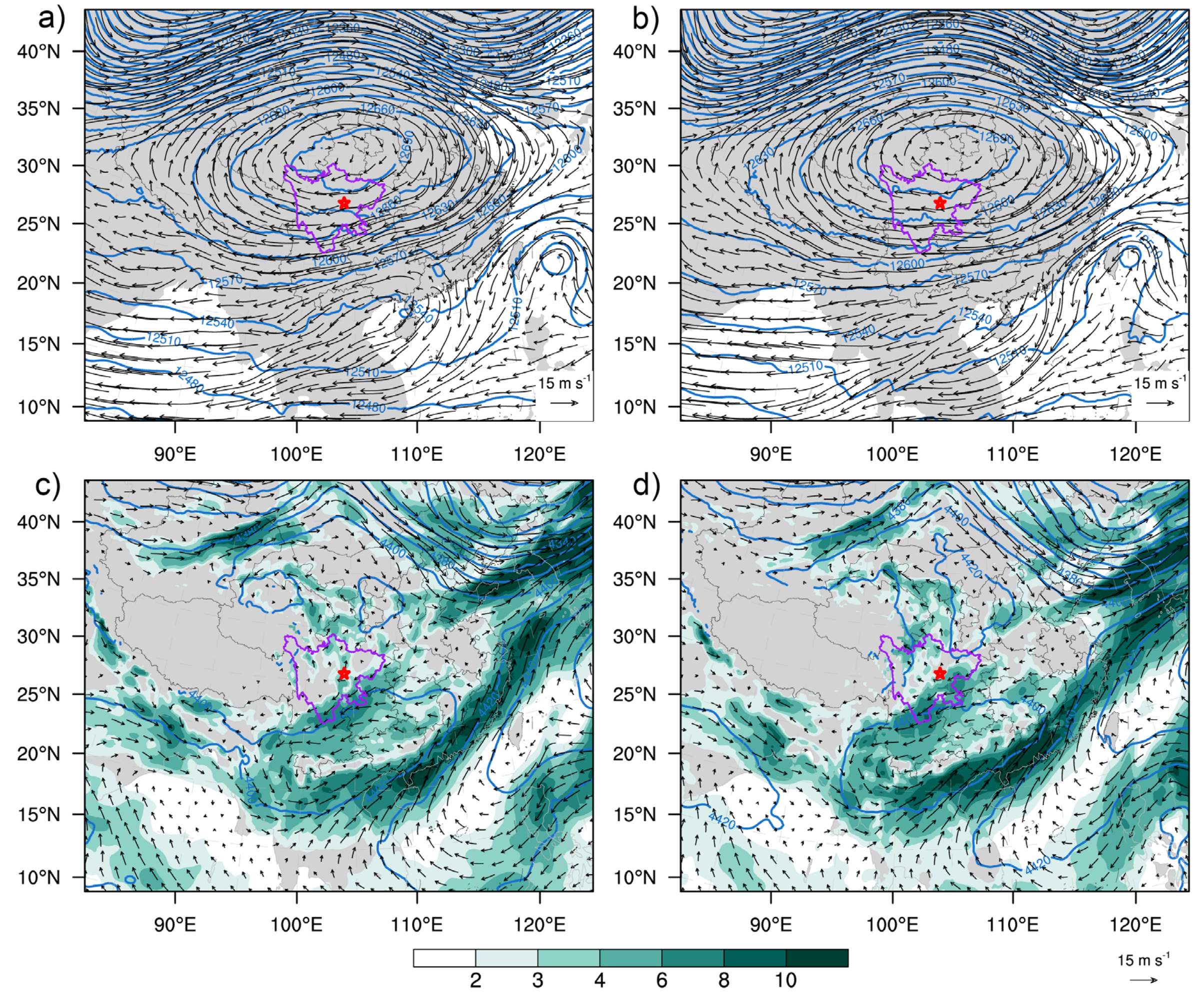

Figure 1: 200 hPa geopotential heights (blue contours, unit: gpm) and horizontal wind field (vectors, unit: m s^{-1}) at (a) 0000 UTC and (b) 0600 UTC. 600 hPa water vapor flux (shaded, units: g s^{-1} hPa^{-1} cm^{-1}), geopotential heights, and horizontal wind field at (c) 0000 UTC and (d) 0600 UTC 6 August 2025. The purple line represents the boundary of Sichuan Province, and the star indicates Chengdu city.

Triggered by these favorable synoptic conditions, convective clouds continuously initiated over the Sichuan region. Radar composite reflectivity shows that initial convection formed east of Chengdu and propagated westward, eventually organizing into multiple convective cloud clusters. The maximum composite radar reflectivity reached approximately 55 dBZ during the mature stage of the event (Fig. 2). Consistent with the radar evolution, surface observations revealed two distinct V-shaped bands of 12-hour accumulated precipitation, primarily associated with the westward propagation of these convective clusters (Fig. 3a).

https://doi.org/10.5194/egusphere-2026-5549
Preprint. Discussion started: 22 September 2026

Overall, this event represents a typical warm-season convective precipitation case in Southwest China, characterized by strong dynamical forcing, abundant moisture supply, and interactions with complex terrain. It therefore provides a suitable meteorological background for conducting case-based cloud seeding experiments.

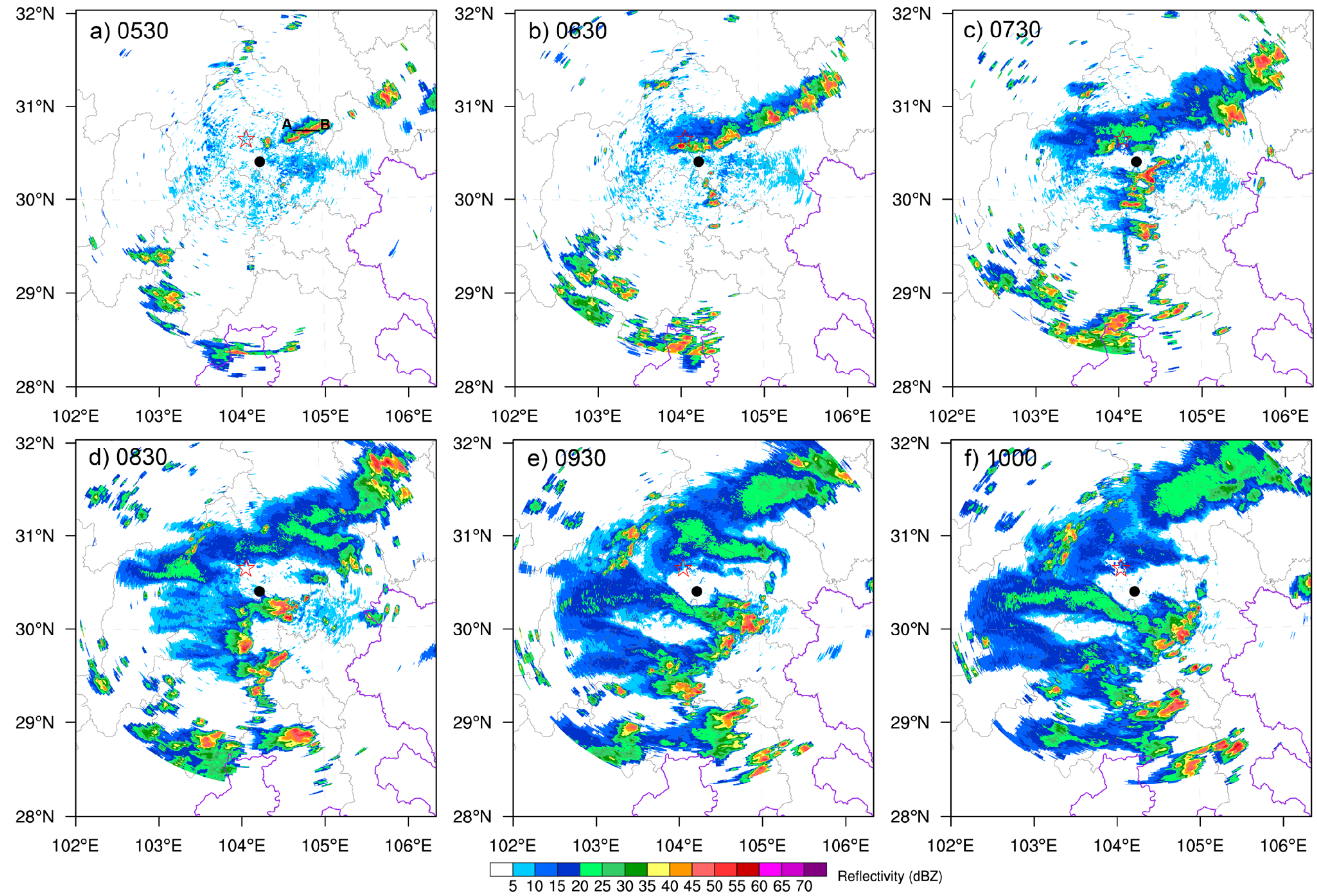

Figure 2: Horizontal distributions of composite radar reflectivity (dBZ) observed by the Chengdu S-band Doppler weather radar station (Z9280; solid black dot) at (a) 0530, (b) 0630, (c) 0730, (d) 0830, (e) 0930, and (f) 1000 UTC 6 August 2025. The star indicates Chengdu city.

The simulated 12-h accumulated precipitation distribution, average and maximum hourly rainfall are generally in good agreement with the observations in d03 of the real-case simulation (Fig. 3). The observed 12-h accumulated precipitation distributes as a V-shaped rain band (Fig. 3a), but the simulation does not reflect the right band well (Fig. 3b). The simulated temporal evolution of average hourly rainfall is well consistent with that observed (Fig.3c), but the simulation produces higher maximum rainfall intensity (Fig.3d). Therefore, the real-case simulation adequately captures the main characteristics of this convective precipitation event, which provides a strong support for a reliable sounding profile extracted from d03 at 0530 UTC 6 August 2025 (position: 30.7°N, 105.1°E) and used for the initialization of the idealized WRF simulations.

https://doi.org/10.5194/egusphere-2026-5549
Preprint. Discussion started: 22 September 2026

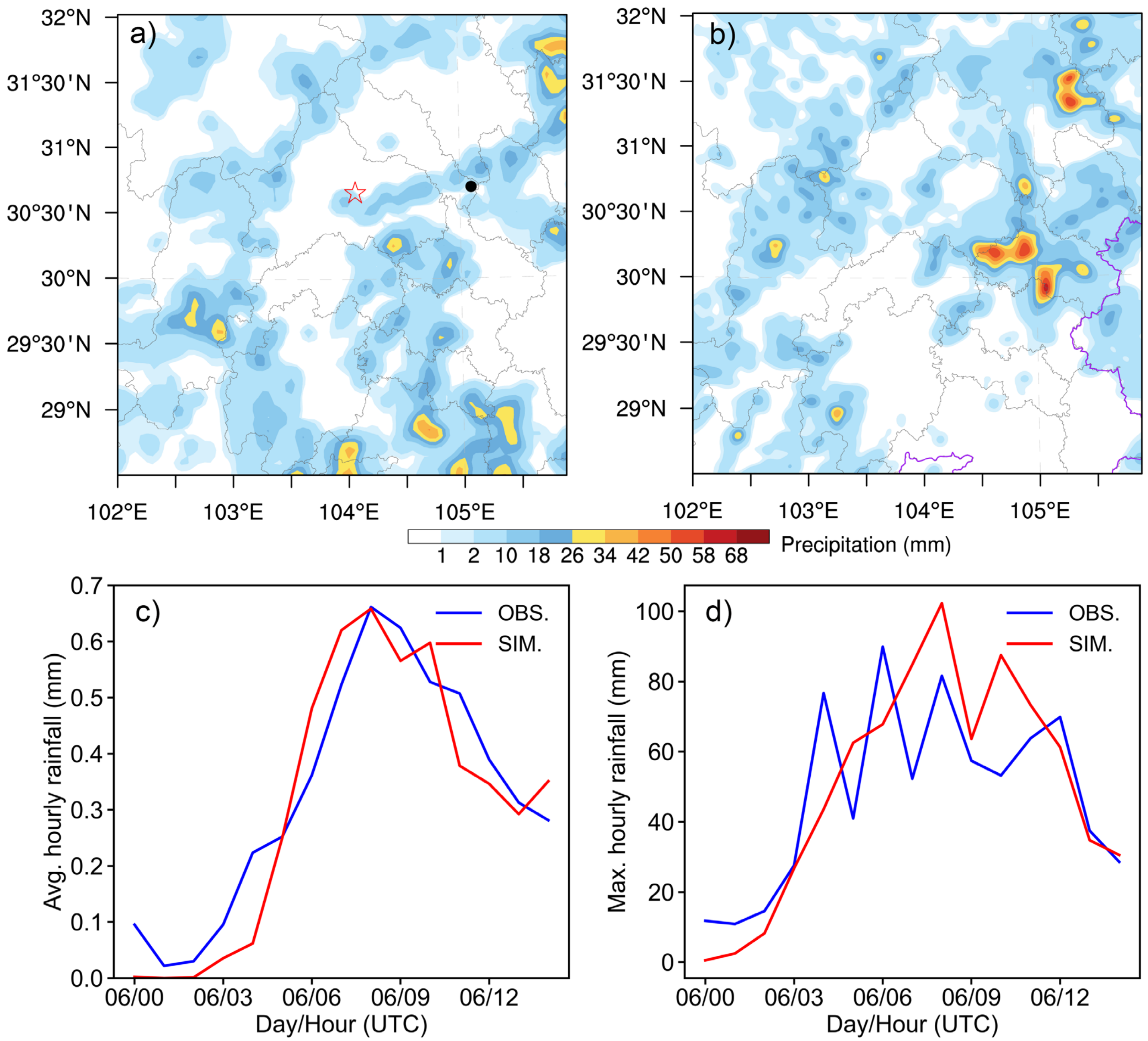

Figure 3: The 12-h accumulated precipitation (color shaded; mm) (a) observed and (b) simulated (d03) in a real-case WRF simulation from 0000 to 1200 UTC 6 August 2025. Time series of regional observed (blue line) and simulated (red line) (c) average and (d) maximum hourly rainfall (mm) in d03. The red star in (a) indicates Chengdu city and the black dots indicate the location where the sounding profile is extracted in Fig. 4.

The extracted sounding profile is shown in Fig. 4. It exhibits wet at 400-500 hPa and relatively dry at upper and lower layers. Precipitable water (PW) is approximately 6 cm. The convective available potential energy (CAPE) is approximately 962 J

https://doi.org/10.5194/egusphere-2026-5549
Preprint. Discussion started: 22 September 2026

kg^{-1}, indicating a moderate thermodynamic instability. The relatively low lifting condensation level (889 hPa) favors convective initiation under an appropriate lifting. In addition, the stronger vertical wind shear from the surface to 600 hPa provides favorable dynamical conditions for the development and maintenance of convection (Chen et al., 2015).

The sounding also shows that the 0 °C level is located at approximately 5.5 km. The LCL is located at 889 hPa, corresponding to an approximate cloud-base height of 1.0 km. Therefore, the warm-cloud layer from the cloud base to the 0 °C level has a depth of approximately 4.5 km, while the cold-cloud layer above the 0 °C level extends for more than 12 km. The deep warm and cold layers provide favorable conditions for active warm and cold rain processes, as well as a suitable condition for testing proposed seeding method. The vertical cross section of radar reflectivity at 0530 UTC shows that the radar echo top reaches approximately 18–20 km (Fig. 5), indicating a well-developed deep convection.

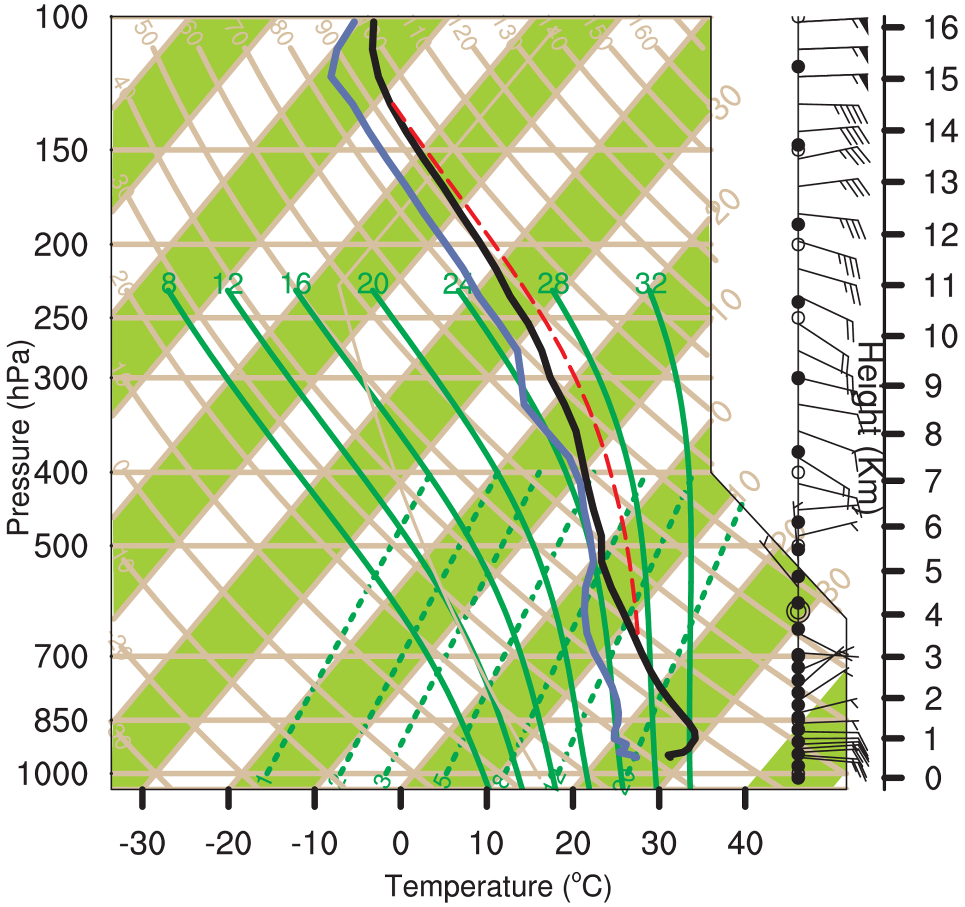

Figure 4: Skew-T diagram of the sounding profiles of temperature (solid black line) and dewpoint temperature (solid blue line) at the position of (30.7°N, 105.1°E) extracted from a real-case WRF simulation at 0530 UTC 6 August 2025. The red dashed line is the atmospheric state curve.

https://doi.org/10.5194/egusphere-2026-5549
Preprint. Discussion started: 22 September 2026

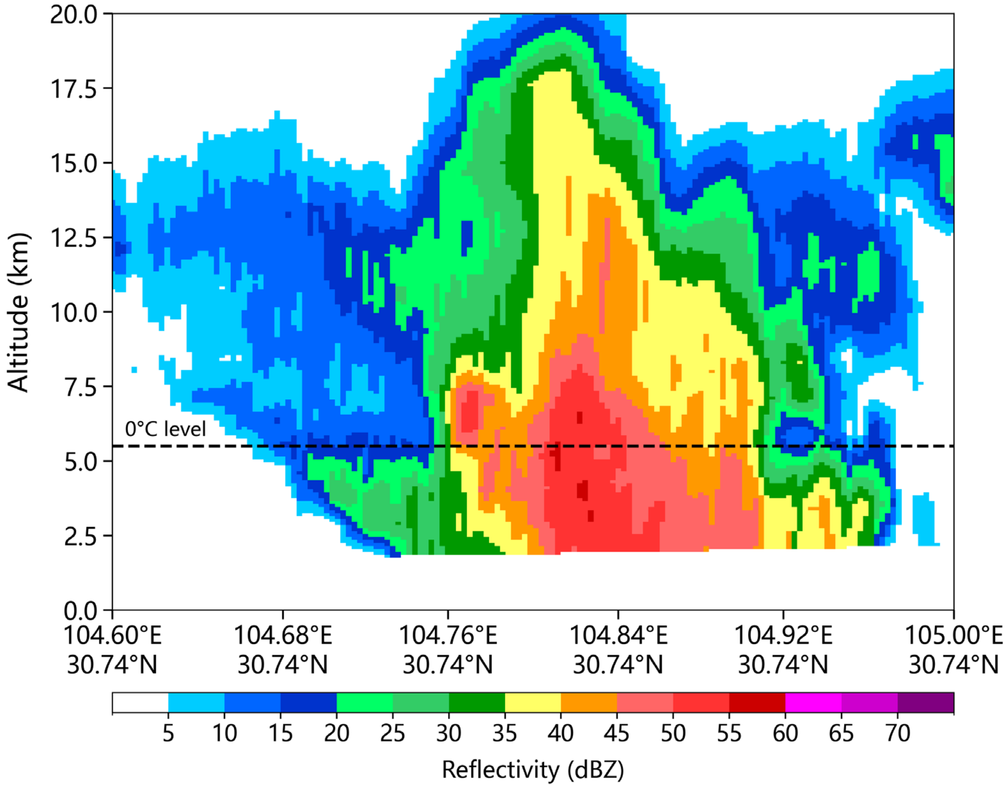

250 **Figure 5**: Vertical cross section of radar reflectivity (dBZ) observed by the Chengdu S-band Doppler weather radar station (Z9280) along 30.74°N at 0530 UTC 6 August 2025. The black dashed line indicates the 0 °C level.

3.2 Setup of seeding experiments

The 64 tests are conducted in this study, including one Control (unseeded) test, seven separate tests with different seeding rates of glaciogenic and hygroscopic agents, and 49 tests for the combination of glaciogenic and hygroscopic cloud seedings with different seeding rates. The setup of seeding experiments is summarized in Table 1.

Previous studies have demonstrated that when glaciogenic cloud seeding with AgI is conducted in regions with abundant supercooled liquid water (SLW) and strong updrafts, and hygroscopic cloud seeding is made in the updraft regions of warm clouds during the initial development stage of the convection, more effective precipitation enhancement can be obtained (Guo et al., 2006, 2007; Rosenfeld et al., 2010; Yang et al., 2024). The seeding time and location are determined in this study based on these previous results. For all seeding tests, the horizontal seeding is conducted within 6 km on both sides of the center point (x, y) = (200, 196) km, with a total length of 12 km. For individual hygroscopic cloud seeding (Fig. 6a, c), the seeding is conducted at altitudes between 2.4 and 4.4 km where are warm clouds with stronger updraft and facilitate hygroscopic CCN activation, condensational and collision–coalescence growth processes. The seeding begins at 10 min and

https://doi.org/10.5194/egusphere-2026-5549
Preprint. Discussion started: 22 September 2026

ends at 40 min, lasting for 30 min. For individual glaciogenic cloud seeding with AgI (Fig. 6b, d), the seeding is made at altitudes between 6.6 and 8.6 km (approximately from −5 °C to −20 °C) where contain abundant SLW with strong updrafts and favor the AgI nucleation. The seeding begins at 30 min and ends at 60 min, lasting for 30 min. For the combined cloud seeding, the seeding time and location are kept unchanged but combine both individual seeding together. The hygroscopic seeding is conducted at the low levels of clouds at first, and then the glaciogenic seeding is made at the upper levels of clouds. The main goal for this combined seeding is to increase the SLW needed for glaciogenic seeding through hygroscopic seeding at an earlier time and lower levels.

Table 1. Setup of seeding experiments

Test type	Seeding rate	Seeding time	Seeding height	Horizontal seeding range	Test number
Control/unseeded	0	—	—	—	1
Glaciogenic seeding/AgI	0.01, 0.05, 0.07, 0.09, 0.10, 0.11, 0.12 g s^{-1}	30–60 min	6.6–8.6 km (−5 to −20 °C)	±6 km from (x, y) = (200, 196) km	7
Hygroscopic seeding/CCN	10^9, 10^{11}, 10^{12}, 10^{13}, 10^{14}, 10^{15}, 10^{16} s^{-1}	10–40 min	2.4–4.4 km (5 to 15 °C)	±6 km from (x, y) = (200, 196) km	7
The combined seeding of CCN + AgI	CCN rates AgI rates	CCN: 10–40 min; AgI: 30–60 min	CCN: 2.4–4.4 km; AgI: 6.6–8.6 km	±6 km from (x, y) = (200, 196) km	49

https://doi.org/10.5194/egusphere-2026-5549
Preprint. Discussion started: 22 September 2026

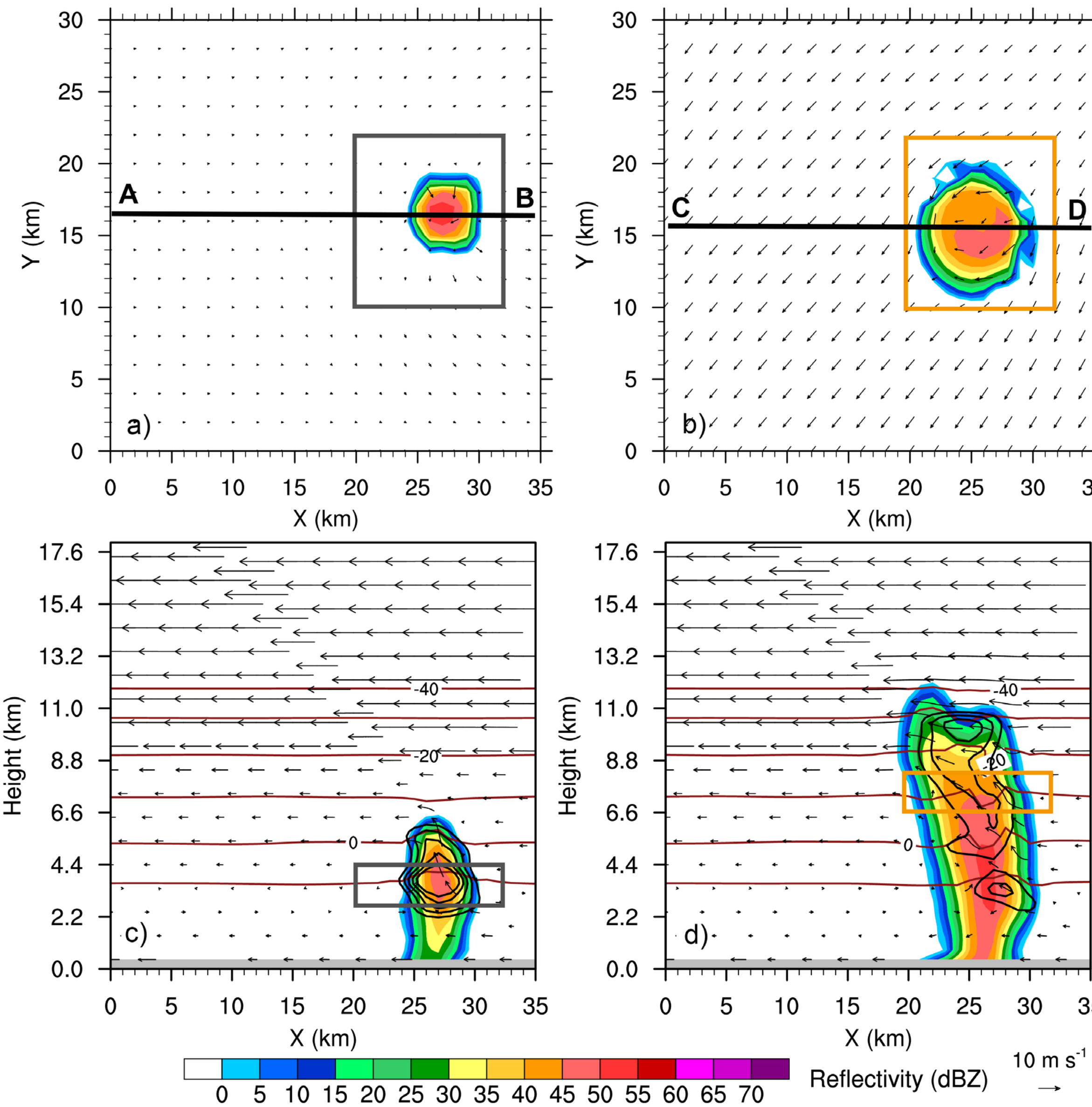

275 **Figure 6**: Horizontal distributions of the simulated radar reflectivity (color shaded; dBZ) and wind field (arrow; m s^{-1}) at (a) 3 km and 20 min and (b) 7 km and 30 min, and (c) and (d) corresponding vertical cross sections along AB and CD lines in (a) and (b) for radar reflectivity (color shaded; dBZ), mixing ratios of cloud water (black solid lines, from 0.4 to 1.2 with an interval of 0.2; g^{-1} kg^{-1}), temperature (red solid lines, from −40 to 10 with an interval of 10; °C), and wind field (arrows; m

280 s^{-1}). The black boxes in (a), (c) denote the hygroscopic seeding location, and the orange boxes in (b), (d) mark the glaciogenic seeding location.

https://doi.org/10.5194/egusphere-2026-5549
Preprint. Discussion started: 22 September 2026

4 Effects of cloud seeding on processes of clouds and precipitation

4.1 Comparisons between the individual and combined cloud seeding approaches

Figure 7 illustrates the sensitivity of the rainfall enhancement rate (RER), defined as the percentage of the accumulated surface rainfall difference between seeded and unseeded relative to that unseeded (control), to various individual glaciogenic and hygroscopic cloud seeding rates. For the individual glaciogenic cloud seeding with AgI agent (Fig. 7a), the RER increases with the AgI seeding rate and reaches the maximum of 7.97% at the seeding rate of 0.09 g s^{-1}, and then it decreases with increasing seeding rate. This nonmonotonic response is consistent with an overseeding effect (Reisin et al., 1996), since the excessive AgI seeding can introduce too many ice nucleating particles (INPs) into the mixed-phase region, intensifying competition for the available water vapor and supercooled liquid water. As a result, a large number of small ice crystals may form, but their growth into precipitation-sized particles is limited, ultimately suppressing the precipitation efficiency.

For the individual hygroscopic cloud seeding with CCN agent (Fig. 7b), the RER also increases with increasing seeding rate and reaches the maximum of 20.74% at a seeding rate of 10^{13} s^{-1}, and then decrease with increasing seeding rate. The similar nonmonotonic response to seeding rate can be attributed to the "Twomey effect" (Twomey 1977), indicating that excessive CCN concentrations lead to the activation of more numerous but smaller cloud droplets. The reduced droplet size can inhibit collision–coalescence and delay warm rain formation. It should be noted here, hygroscopic seeding produces a larger RER than glaciogenic seeding, suggesting that warm microphysics may play a more important role in this convective rainfall case.

https://doi.org/10.5194/egusphere-2026-5549
Preprint. Discussion started: 22 September 2026

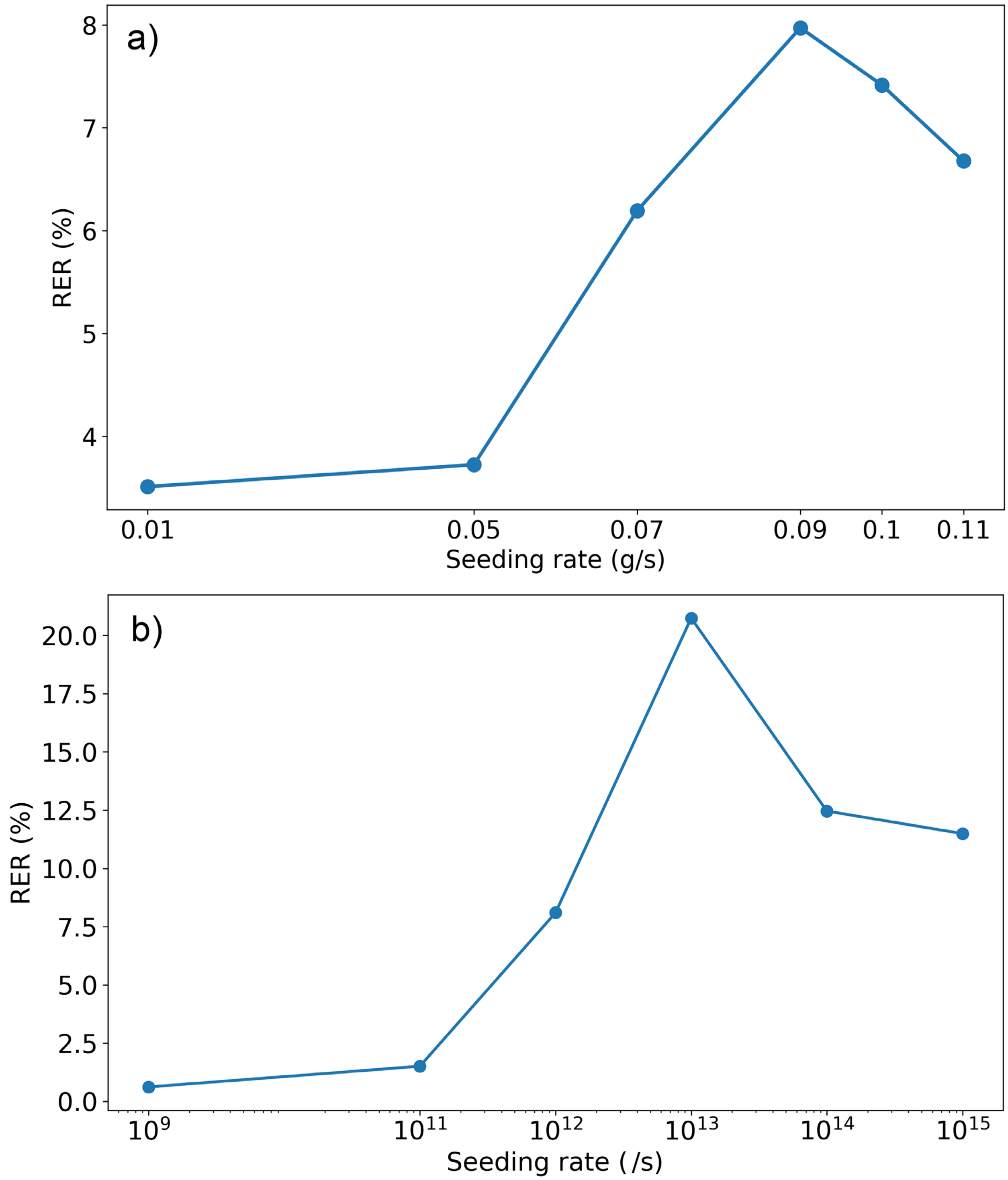

300 **Figure 7**: The sensitivity of the 4-hour accumulated rainfall enhancement rate (RER, %) to various seeding rates for (a) glaciogenic cloud seeding with AgI and (b) hygroscopic CCN seeding.

https://doi.org/10.5194/egusphere-2026-5549
Preprint. Discussion started: 22 September 2026

Figure 8 presents a heatmap of the RER matrix for the individual and combined cloud seeding. The matrix shows that combined cloud seeding can produce substantially larger precipitation enhancement than the individual glaciogenic AgI and hygroscopic CCN seeding. The maximum RER reaches 69.72% under the seeding rate of 0.11 g s^{-1} for AgI and 10^{15} s^{-1} for CCN. Under the conditions with the optimal seeding rate of 0.09 g s^{-1} for individual seeding with AgI and 10^{13} s^{-1} for that with CCN, the RER reaches 57.00%, which is considerably larger than the simple sum of the individual RER (7.97%+20.74%=28.71%), indicating that the combined seeding may produce strong nonlinear dynamical and microphysical responses rather than simple additive responses to convective precipitation. Note, as the CCN seeding rate increases from 10^{13} to 10^{14} s^{-1}, the RER in the combined seeding increases rapidly, indicating that the early hygroscopic seeding with CCN can significantly enhance the subsequent glaciogenic seeding effect with AgI through interactions between warm and cold cloud processes.

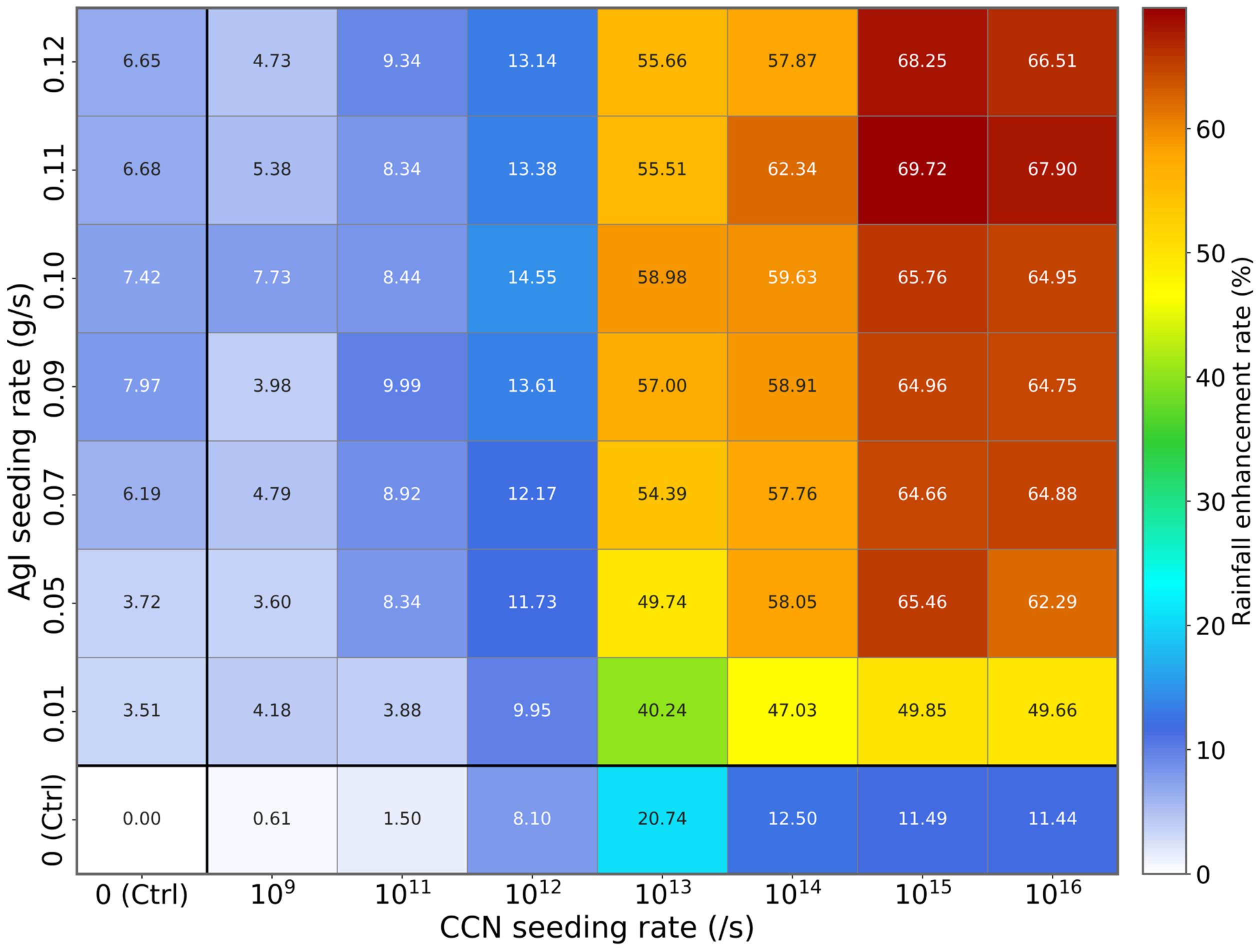

Figure 8: Heatmap of 4-h accumulated rainfall enhancement rate (RER, %) for the individual and combined seeding. The horizontal axis represents the CCN seeding rate (s^{-1}), and the vertical axis denotes the AgI seeding rate (g s^{-1}). The bottom-left cell (0, 0) represents the unseeded control experiment. Numbers in the grid cells are RER.

https://doi.org/10.5194/egusphere-2026-5549
Preprint. Discussion started: 22 September 2026

The comparison is made among unseeded (control), the individual and the combined seeded experiments for the surface rainfall with optimal seeding rates of 10^{13} s^{-1} for CCN and 0.09 g s^{-1} for AgI (Fig. 9). The surface rainfall develops rapidly in 20 min in all experiments. However, comparing to unseeded control experiment, the rainfall volume for the individual AgI seeding weakens at 40-70 min and strengthens after 70 min, whereas that for both the individual hygroscopic seeding and the combined seeding increases from 50 min (Fig. 9a). In contrast, the peak of rainfall volume rate for AgI seeding is suppressed but that for both the CCN and combined seeding is enhanced relative to the control experiment (Fig. 9b). However, the rainfall volume rate for AgI seeding is rapidly enhanced after 60 min, even exceeds the CCN seeding. The interesting phenomenon is that the combined seeding significantly extends the duration the high rainfall rate. The mechanisms behind will be investigated later.

https://doi.org/10.5194/egusphere-2026-5549
Preprint. Discussion started: 22 September 2026

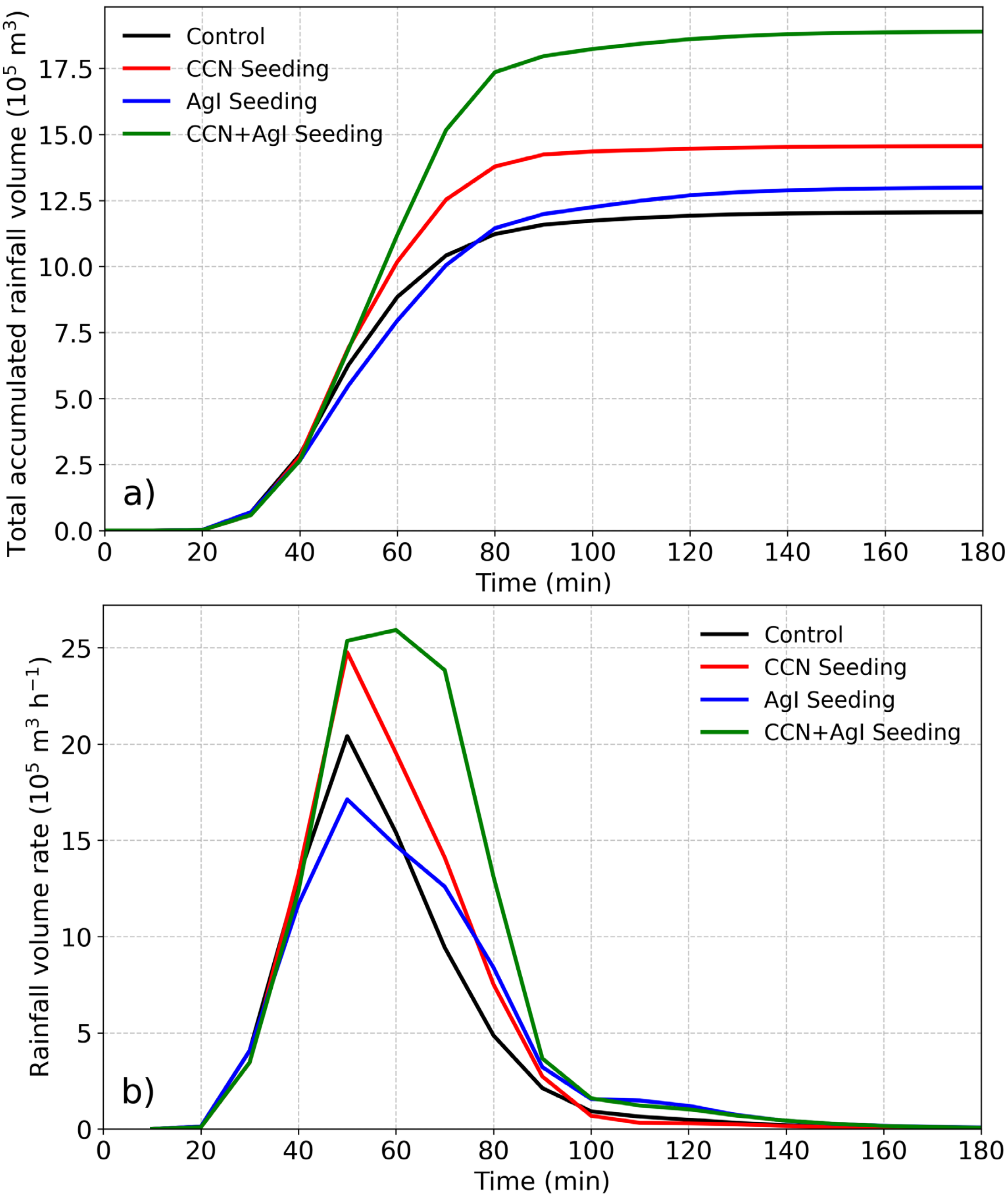

Figure 9: Temporal evolution of domain-integrated (a) accumulated surface rainfall volume (10^5 m^3) and (b) rainfall volume rate (10^5 m^3 h^{-1}) for the experiments of Control, CCN seeding with a rate of 10^{13} s^{-1}, AgI seeding with a rate of 0.09 g s^{-1},
330 and their combined seeding (CCN+AgI).

https://doi.org/10.5194/egusphere-2026-5549
Preprint. Discussion started: 22 September 2026

4.2 The associated physical mechanisms

4.2.1 From cloud microphysical perspective

It is showed that cloud water has two high centers, one larger center is located in the upper cold cloud layers as the supercooled cloud water, and the other smaller one is located in the low warm cloud layers as the warm cloud water in the control experiment (Fig. 10a). The individual CCN seeding significantly enhances cloud water in the whole clouds (Fig. 10b). The most important thing is that the maximum supercooled cloud water at high altitudes is doubled comparing to the control experiment, indicating that CCN seeding in the low warm cloud layers can greatly enhance the supercooled cloud water in the upper cold cloud layers through updraft transport, providing a more favorable condition for the subsequent AgI seeding. The cloud water condensation rate further shows that the CCN seeding enhances cloud water formation during the developing stage, with a larger and longer-lasting cloud condensation rate than that in the control experiment (Fig. 11). The individual AgI seeding leads to a rapid reduction in the supercooled cloud water comparing to the control experiment (Fig. 10c), accompanied by a faster decrease in the cloud water condensation rate after 30 min (Fig. 11). The combined seeding with both AgI and CCN exhibits rapid depletion of the supercooled cloud water (Fig. 10d). The cloud water condensation rate is strongly enhanced before 30 min due to the early CCN seeding, but it rapidly decreases after the AgI seeding (Fig. 11). Therefore, the early CCN seeding during 10–40 min significantly increases the SLW, and the subsequent AgI seeding during 30–60 min rapidly consumes the SLW, resulting in more precipitation at the surface.

https://doi.org/10.5194/egusphere-2026-5549
Preprint. Discussion started: 22 September 2026

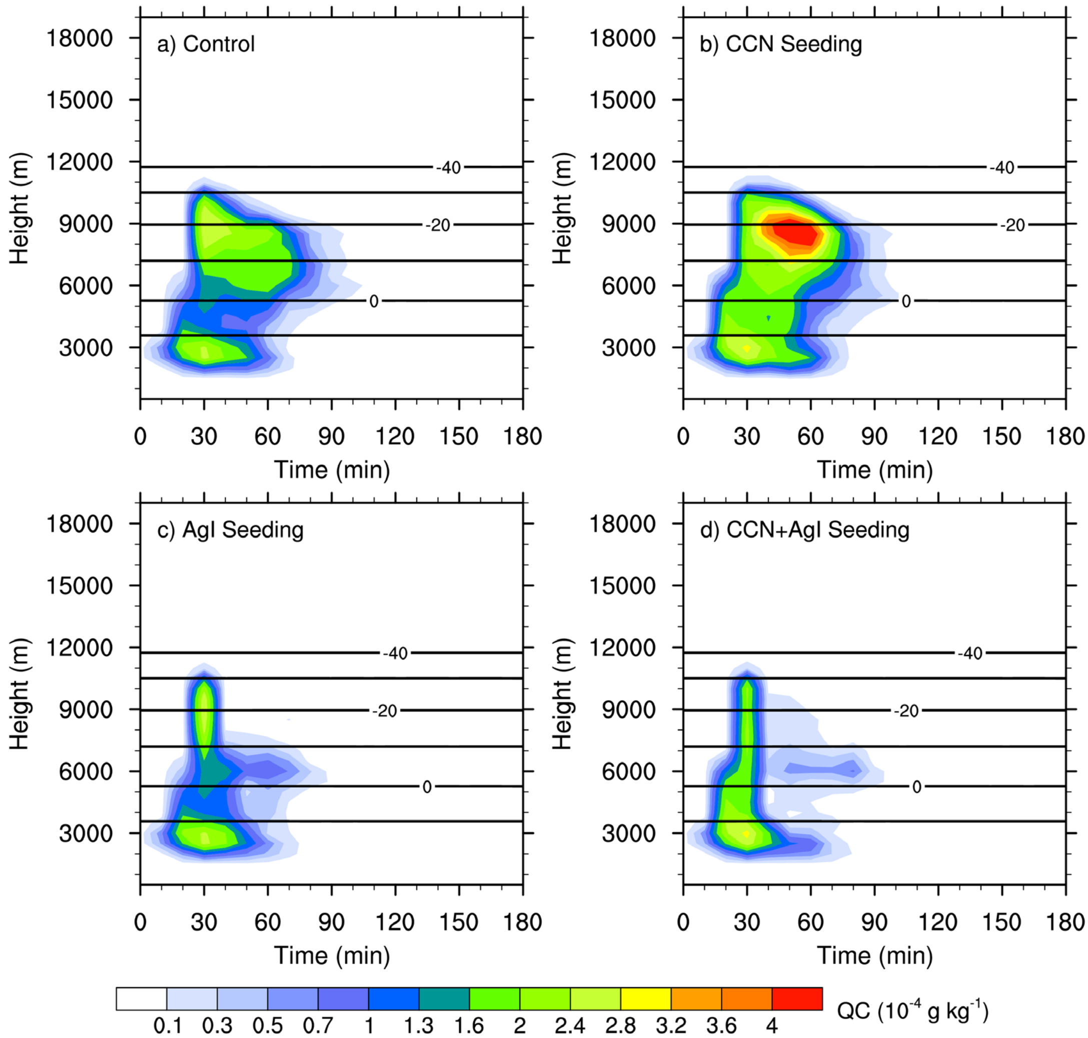

Figure 10: Time-height distribution of the domain-averaged cloud water mixing ratio (color shading, g/kg) and temperature (black solid lines, °C) for experiments of (a) Control, (b) CCN seeding, (c) AgI seeding, and (d) the combined CCN+AgI seeding.

https://doi.org/10.5194/egusphere-2026-5549
Preprint. Discussion started: 22 September 2026

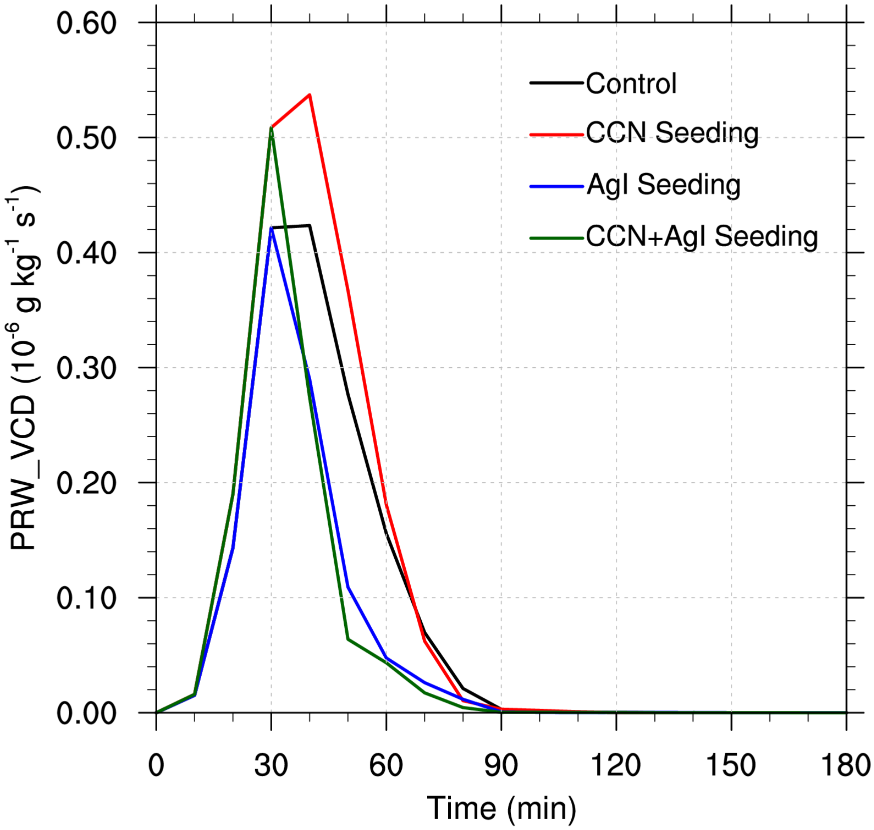

Figure 11: Temporal evolution of the domain-averaged cloud water condensation rate in four experiments.

Cloud ice is distributed in the upper troposphere around 15 km in the control experiment (Fig. 12a). The individual hygroscopic CCN seeding significantly increases cloud ice in the upper levels (Fig. 12b), whereas the individual glaciogenic seeding with AgI has no apparent effect on cloud ice at 15 km but generate cloud ice around 7– 11 km (Fig. 12c). In contract, the combined cloud seeding has both features in the individual hygroscopic and glaciogenic seeding, cloud ice apparently increases in both 7–11 km and 15 km (Fig. 12d). The source terms of cloud ice show that it is primarily converted from water vapor deposition process (PRI_IDE) and cloud water freezing process (PRI_WFZ) has less contribution in the control experiment (Fig.13a). The hygroscopic CCN seeding slightly enhances conversion rates of both PRI_IDE and PRI_WFZ processes (Fig. 13b), because the condensational nucleating cloud droplets can be transported to the upper layers by updraft and freeze as cloud ice, leading to an increase in cloud ice in the upper layers. The glaciogenic cloud seeding with AgI directly adds artificial ice nucleation process (PRI_INU) and markedly increase PRI_IDE (Fig. 13c). The combined seeding increases cloud ice more apparently through processes of PRI_IDE, PRI_INU and PRI_WFZ through utilizing advantages in individual cloud seeding (Fig. 13d).

https://doi.org/10.5194/egusphere-2026-5549
Preprint. Discussion started: 22 September 2026

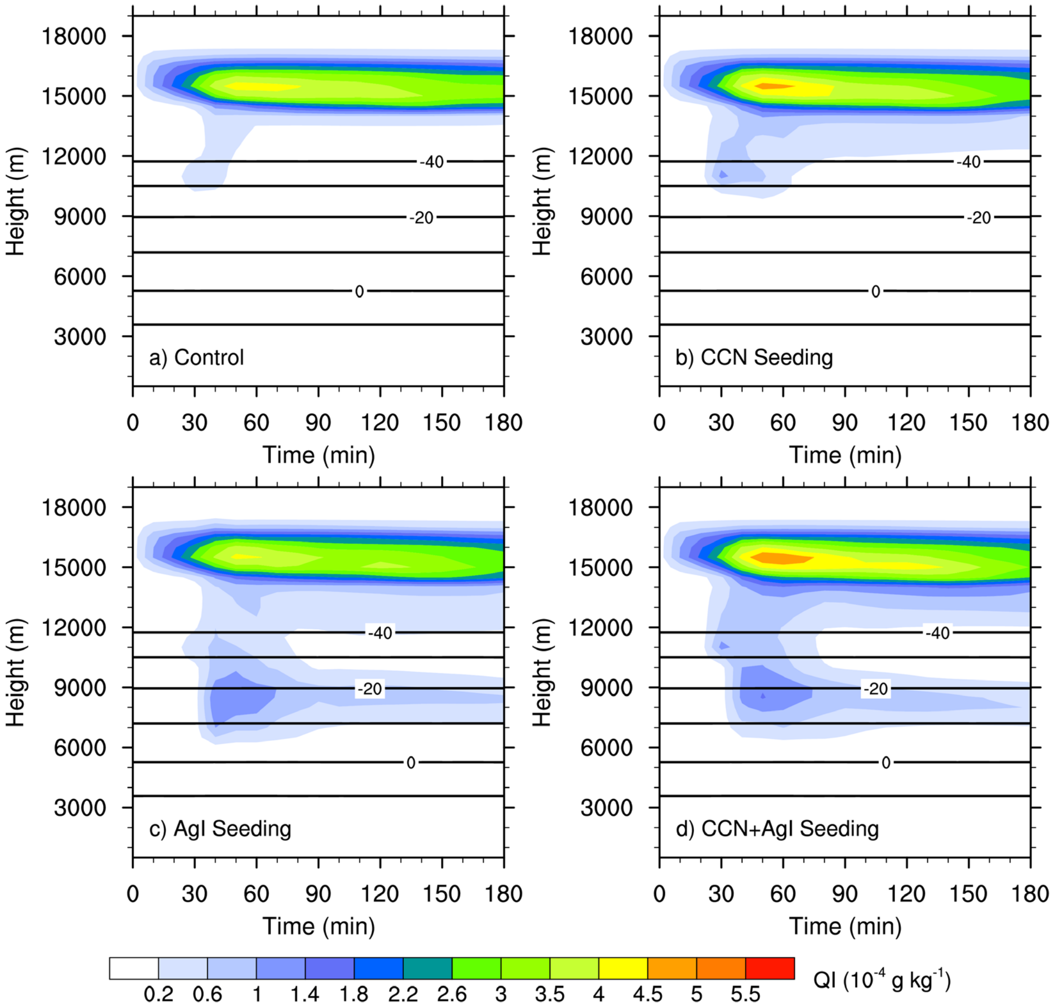

Figure 12: As in Fig. 10, but for cloud ice mixing ratio.

https://doi.org/10.5194/egusphere-2026-5549
Preprint. Discussion started: 22 September 2026

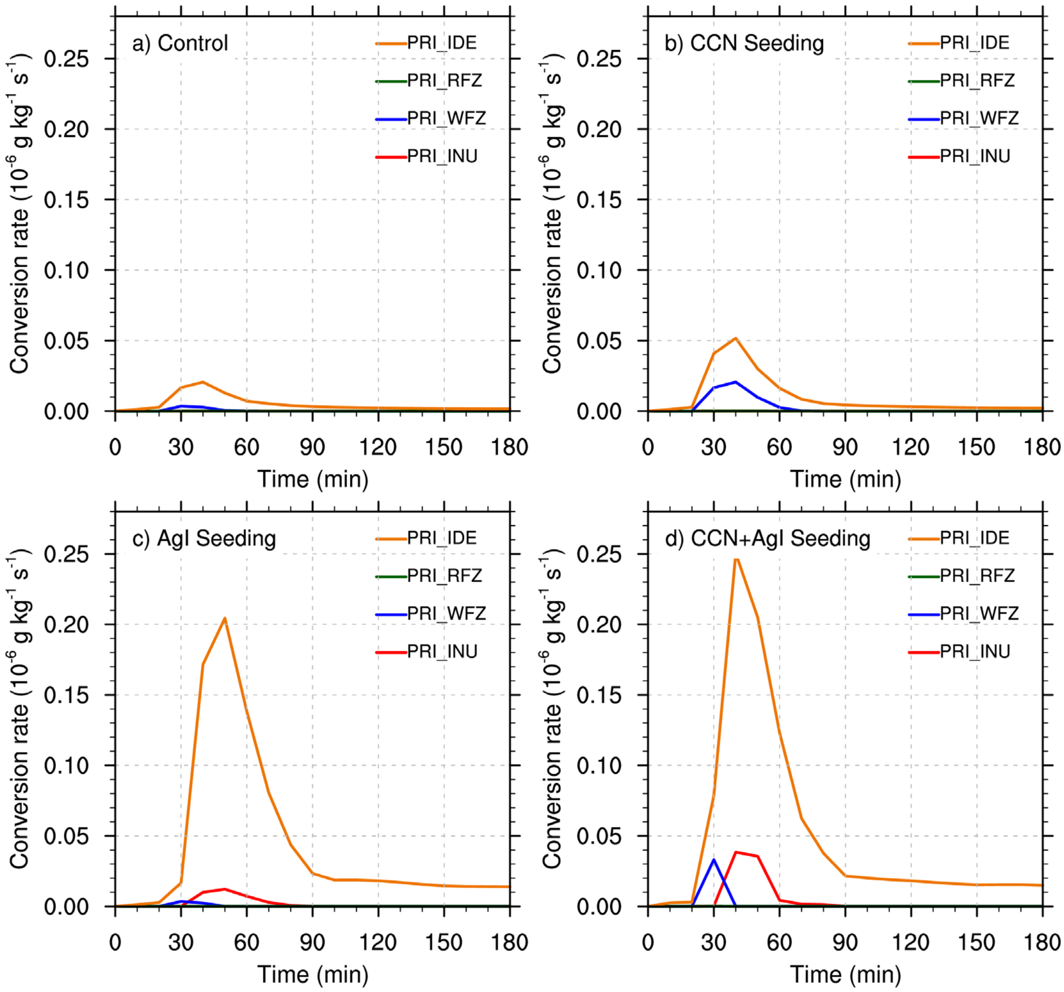

Figure 13: Temporal evolution of the domain-averaged conversion rates for cloud ice source terms in experiments of (a) Control, (b) CCN seeding, (c) AgI seeding, and (d) the combined CCN+AgI seeding.

Snow has two centers at 8 and 15 km in the control experiment (Fig. 14a). The individual hygroscopic CCN seeding increases snow in the upper layers around 15 km (Fig. 14b), and the glaciogenic AgI seeding distinctly enhances the amount and vertical distribution of snow (Fig. 14c). The combined seeding can produce more snow in the upper layers than the AgI seeding (Fig. 14d). The source terms of snow show that it is produced through the processes of autoconversion of cloud ice (PRS_IAU), vapor deposition (PRS_SDE) and accretion of the supercooled cloud water (PRS_SCW) in the control experiment (Fig. 15a). The hygroscopic CCN seeding strengthens the PRS_IAU process but weakens the PRS_SDE process owning to that the seeding increases cloud ice in the upper layer (Fig. 15b), whereas the glaciogenic AgI seeding substantially increases artificial cloud ice and enhances processes of PRS_IAU and PRS_SDE (Fig. 15c). The combined

https://doi.org/10.5194/egusphere-2026-5549
Preprint. Discussion started: 22 September 2026

CCN+AgI seeding significantly enhances both PRS_SDE and PRS_IAU comparing with CCN seeding, and PRS_SDE comparing with AgI seeding (Fig. 15d).

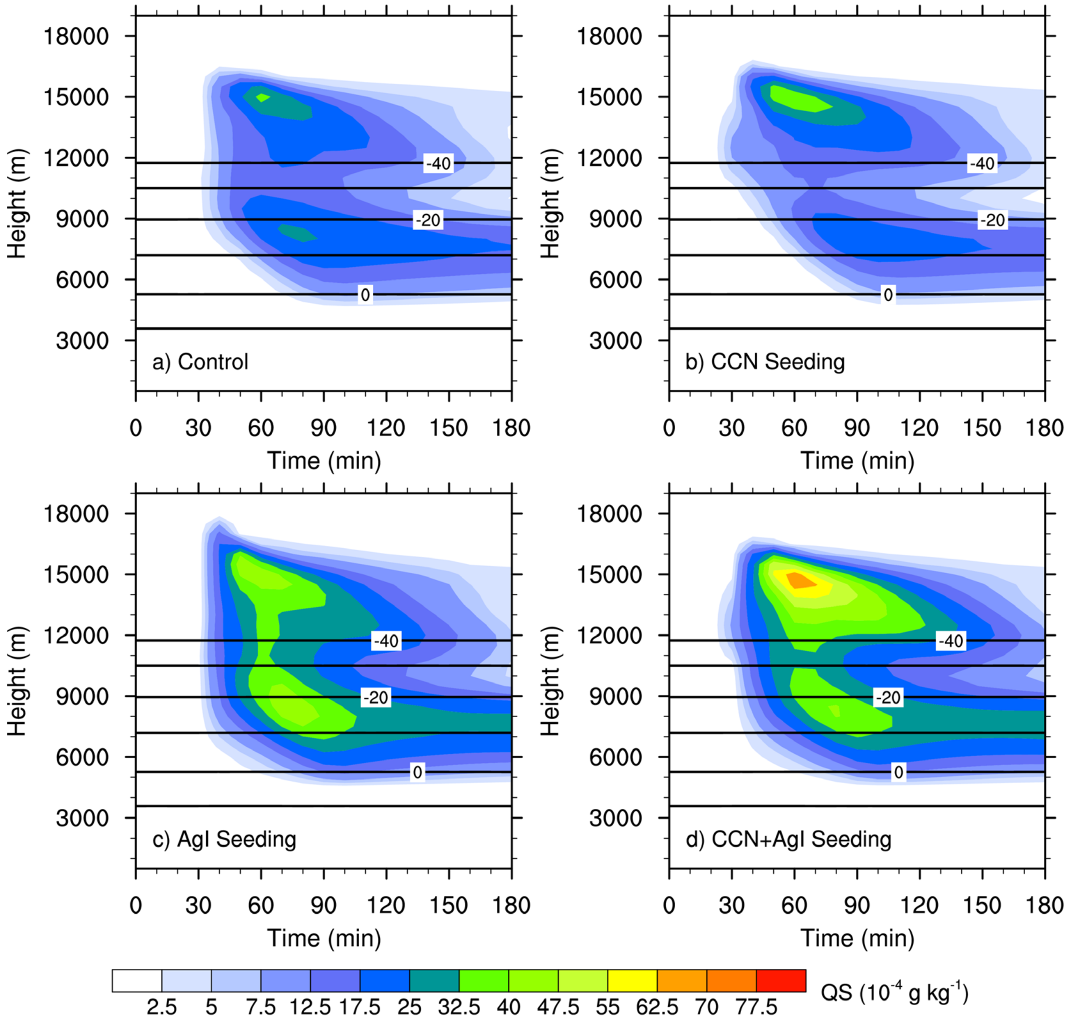

385 **Figure 14**: As in Fig. 10, but for snow mixing ratio.

https://doi.org/10.5194/egusphere-2026-5549
Preprint. Discussion started: 22 September 2026

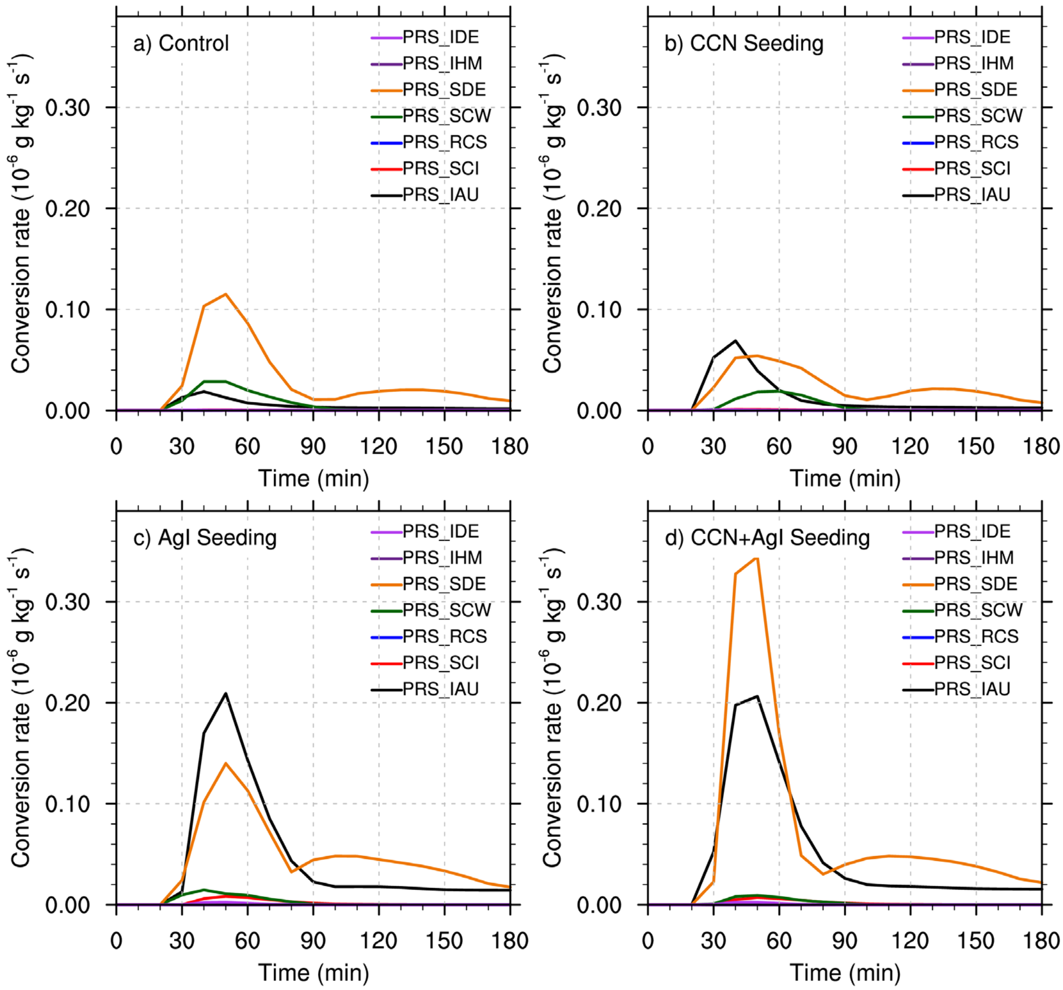

Figure 15: As in Fig. 13, but for snow source terms.

Graupel is primarily located at 5–11 km with a maximum mixing ratio of 8×10^{-4} g/kg at around 7 km in the control experiment (Fig. 16a). The hygroscopic cloud seeding with CCN substantially increases graupel mixing ratio up to 1.2×10^{-3} g/kg, vertical distribution to 15 km and duration comparing to the control experiment (Fig. 16b), whereas the glaciogenic cloud seeding with AgI does not increase graupel mixing ratio as obviously as the CCN seeding, but its vertical range and duration are also increased comparing to the control experiment (Fig. 16c). However, the combined seeding significantly increase graupel mixing up to 1.6×10^{-3} g/kg, and the vertical distribution range and duration are also obviously extended (Fig. 16d).

Graupel source terms show that graupel is mainly converted from processes of collection of cloud ice by the supercooled rainwater (PRG_RCI), collection of the supercooled cloud water (PRG_GCW) and rainwater (PRG_RCG) by graupel in the control experiment (Fig. 17a). Comparing to the control experiment, the hygroscopic CCN seeding significantly enhances

https://doi.org/10.5194/egusphere-2026-5549
Preprint. Discussion started: 22 September 2026

processes of PRG_GCW and collection of ice crystal by rainwater and conversion to graupel (PRG_RCI) because of the increased supercooled cloud water and rainwater (Fig. 17b), while the glaciogenic AgI seeding mainly enhances the conversation processes from the supercooled rainwater by snow (PRG_RCS) and graupel deposition (PRG_GDE) (Fig. 17c), reflecting the strengthened ice-phase process. The combined seeding enhances conversion processes of PRG_RCS, PRG_RCI and PRG_GCW, indicating that both liquid-phase and ice-phase processes are enhanced (Fig. 17d).

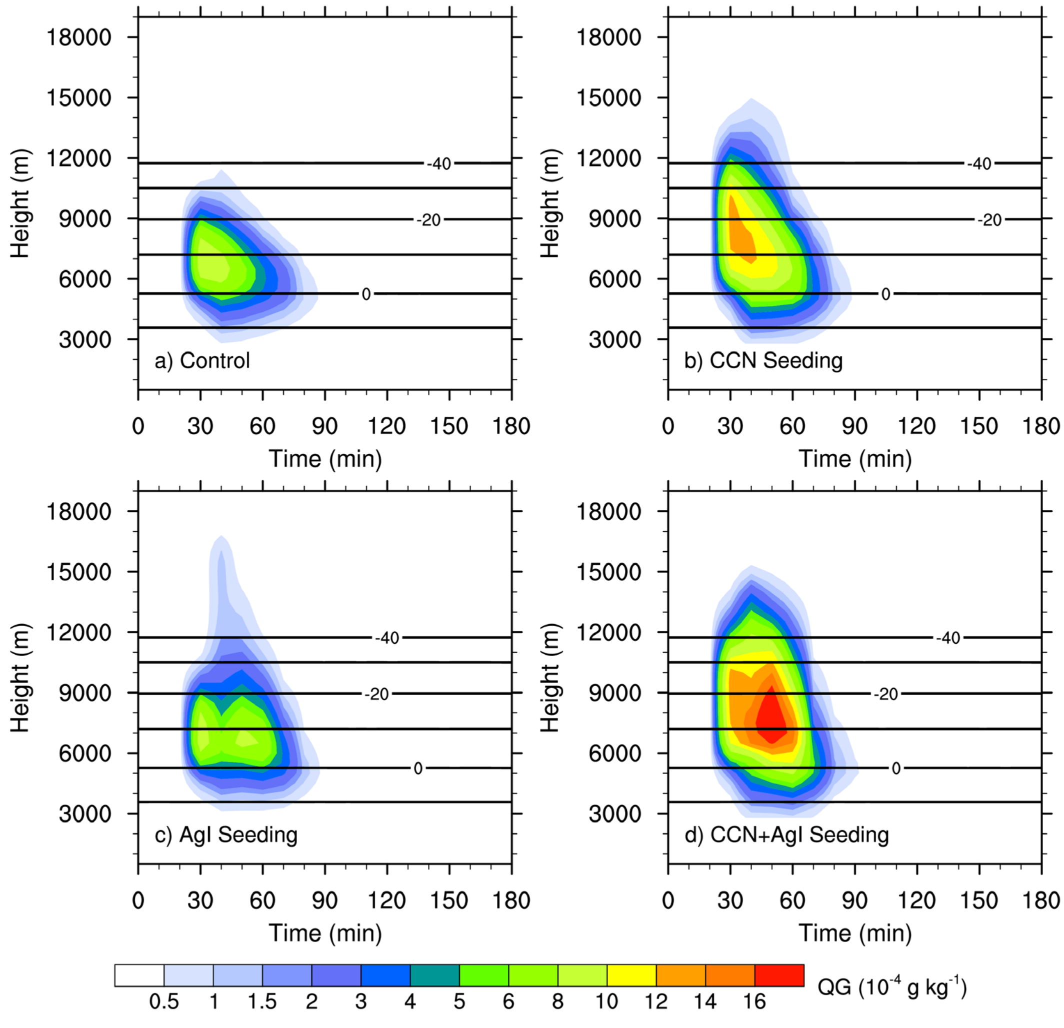

Figure 16: As in Fig. 10, but for graupel mixing ratio.

https://doi.org/10.5194/egusphere-2026-5549
Preprint. Discussion started: 22 September 2026

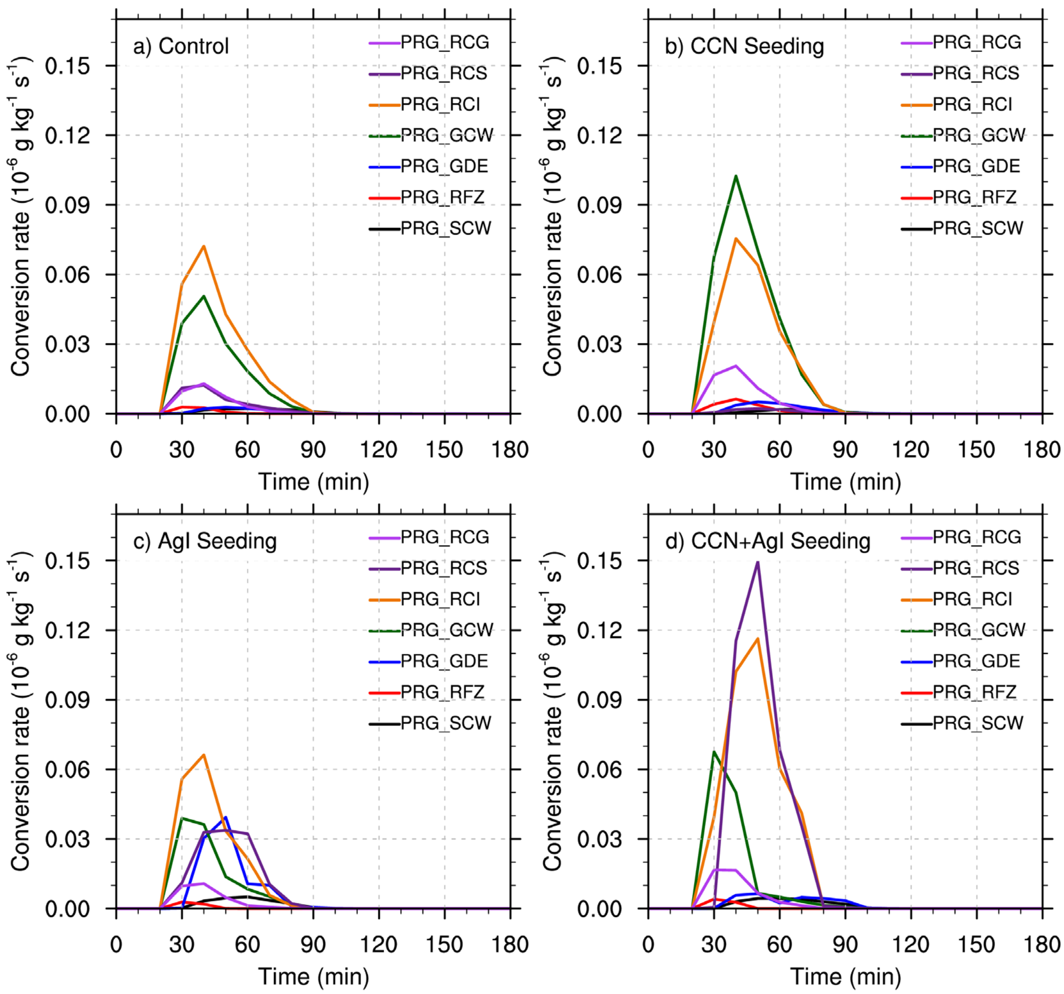

Figure 17: As in Fig. 13, but for graupel source terms.

Rainwater is mainly distributed below 5 km and exhibits convective vertical distribution at 30–50 min, and then follows a weak stratiform distribution in the control experiment (Fig. 18a). Comparing to the control experiment, the hygroscopic CCN seeding apparently enhances rainwater content and vertical distribution (Fig. 18b), and the glaciogenic AgI seeding slightly suppresses the maximum rainwater content in the early stage but enhances in the later stage (Fig. 18c). The combined cloud seeding markedly enhances rainwater volume, maximum content and duration (Fig. 18d).

Rainwater source terms shows that rainwater is converted through processes of autoconversion of cloud water to rainwater (PRR_WAU), collision-coalescence (PRR-RCW) and melting of graupel (PRR_GML) and snow (PRR_SML) in the control experiment (Fig. 19a). Comparing to the control experiment, the hygroscopic CCN seeding produces much more but smaller cloud droplets, leading to a suppression of PRR_WAU, but significantly enhances processes of PRR_RCW and PRR_GML (Fig. 19b), whereas the glaciogenic AgI seeding produces more cloud ice, and primarily enhances PRR_SML through the

https://doi.org/10.5194/egusphere-2026-5549
Preprint. Discussion started: 22 September 2026

depletion of the supercooled cloud water (Fig. 19c). The combined cloud seeding fully utilizes advantages of both hygroscopic and glaciogenic seeding and markedly enhances processes of PRR_GML, PRR_SML and PRR_RCW, resulting in an obvious increase of rainwater content and duration (Fig. 19d).

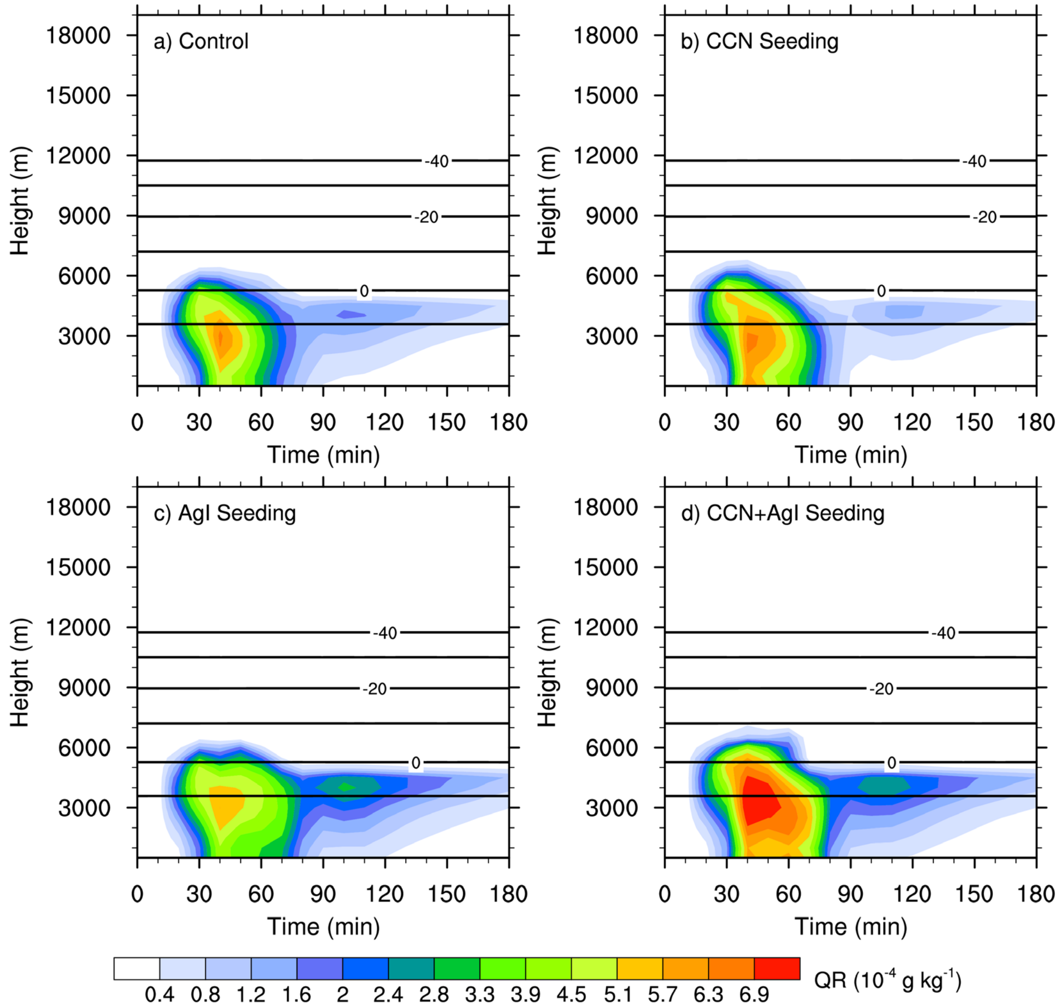

425

Figure 18: As in Fig. 10, but for rainwater mixing ratio.

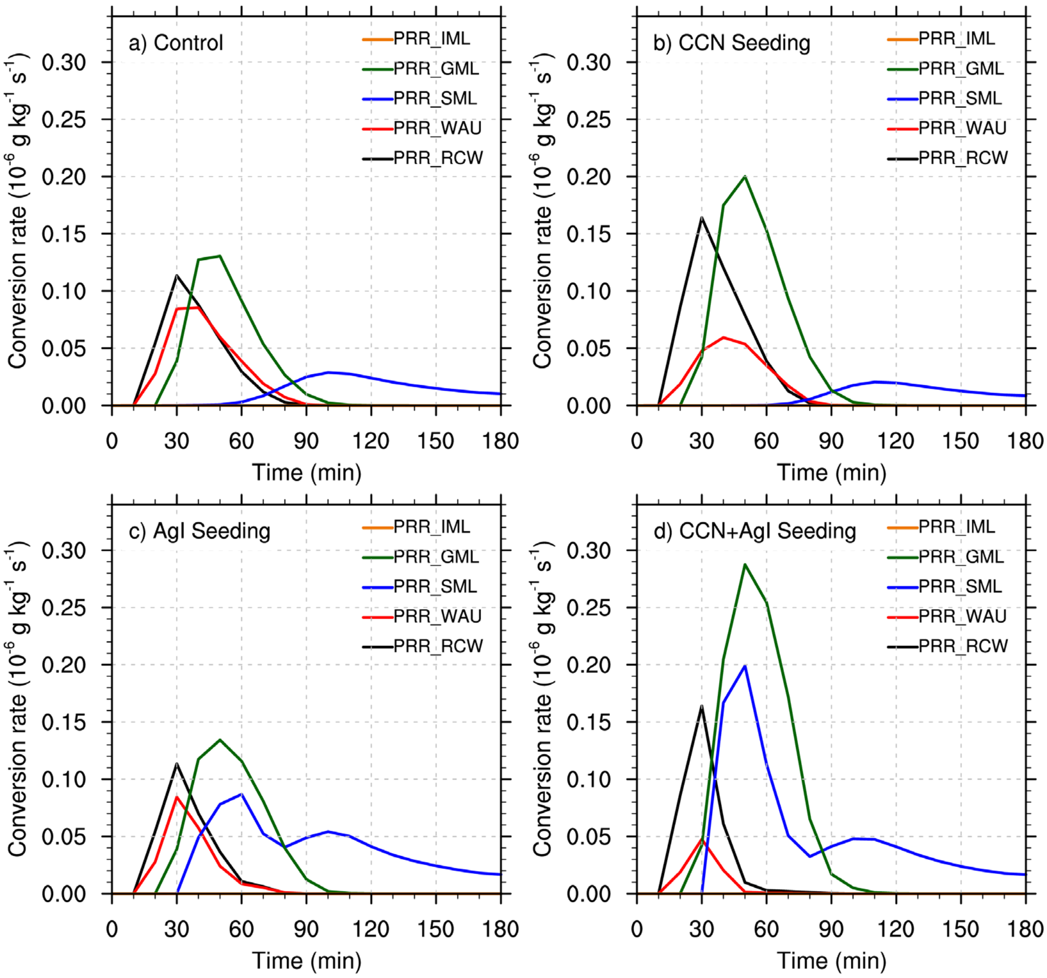

Figure 19: As in Fig. 13, but for rainwater source terms.

Cloud water path (CWP) and ice water path (IWP) are two important parameters representing cloud liquid and ice properties. For CWP (Fig. 20a), the domain-averaged CWP has a peak value of about 0.85 g m^{-2} at around 40 min in the control experiment. Comparing to the control experiment, the hygroscopic CCN seeding substantially increases the CWP peak up to 1.15 g m^{-2}, since the increase of CCN may enhance cloud water, and result in more CWP. The glaciogenic AgI seeding rapidly deplete the supercooled cloud water and leads to the decrease of CWP. In the combined cloud seeding, the early CCN seeding significantly increases the SLW and the subsequent AgI seeding consumes the SLW, leading an early decrease of CWP.

For IWP (Fig. 20b), the domain-averaged IWP reach a peak value of 7.5 g m^{-2} shows at around 75 min in the control experiment. The hygroscopic CCN seeding causes the earlier formation of IWP than the control experiment. Both AgI seeding and the combined seeding produce a pronounced increase in IWP and the IWP increase is more prominent in the

https://doi.org/10.5194/egusphere-2026-5549
Preprint. Discussion started: 22 September 2026

combined seeding. Therefore, hygroscopic CCN seeding can increase CWP, and glaciogenic AgI seeding can promote the conversion of supercooled liquid water into ice-phase particles, increasing IWP, the combined cloud seeding is more efficient to enhance liquid-ice conversion processes.

As described above, the proposed combined hygroscopic and glaciogenic cloud seeding can produce much stronger cloud microphysical changes than the individual seeding. The early low-level hygroscopic CCN seeding produces massive cloud droplets and significantly enhances collision-coalescence process, and the formation of SLW and graupel in the upper mixed-phase layer because of strong updraft transport. The subsequent glaciogenic AgI seeding further enhances the glaciation process of SLW and the formation of snow. As a result, processes of graupel and snow melting and collision-coalescence are significantly enhanced and more rainwater is formed.

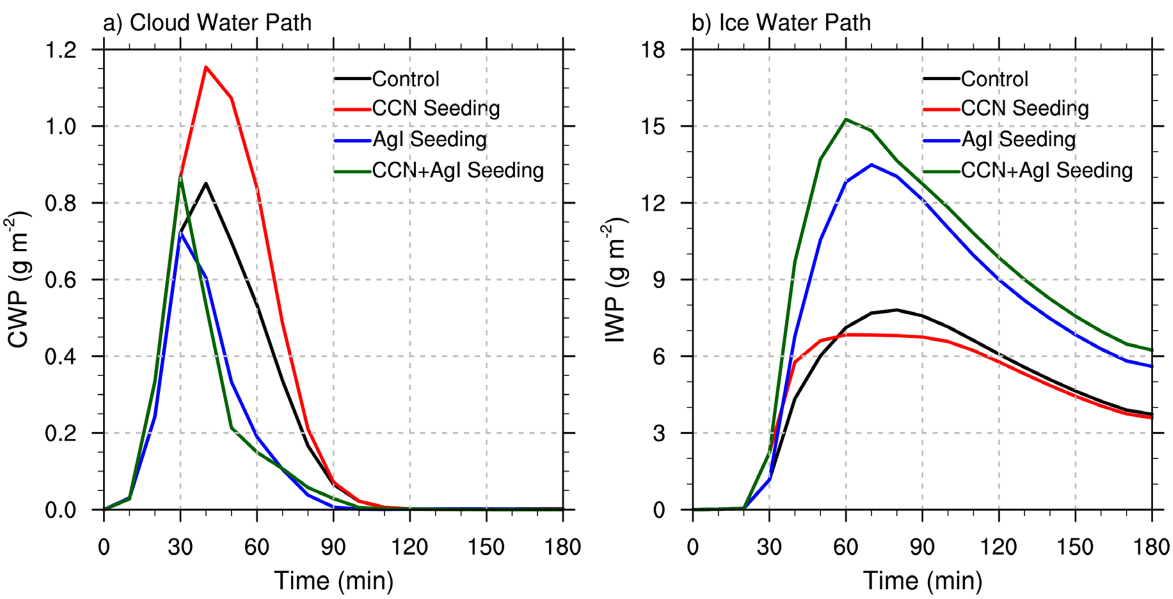

Figure 20: Temporal evolution of domain-averaged (a) cloud water path (CWP) and (b) ice water path (IWP) for experiments of Control, hygroscopic CCN seeding, glaciogenic AgI seeding, and the combined CCN+AgI seeding.

4.2.2 From cloud dynamical perspective

Two updraft cores located at near 7 and 13.5 km appear and the maximum updraft is 20.5 m s^{-1} in the control experiment (Fig. 21a). In contrast, the hygroscopic CCN seeding enhances updraft to become deeper and stronger owning to higher latent heat release induced by CCN seeding and the maximum updraft reaches 24.5 m s^{-1} (Fig. 21b), whereas the glaciogenic AgI seeding also strengthens updraft but not as obvious as CCN seeding (Fig. 21c). The combined cloud seeding produces the strongest updraft with the maximum updraft of 36.5 m s^{-1} (Fig. 21d), since much more latent heat release in the combined seeding.

https://doi.org/10.5194/egusphere-2026-5549
Preprint. Discussion started: 22 September 2026

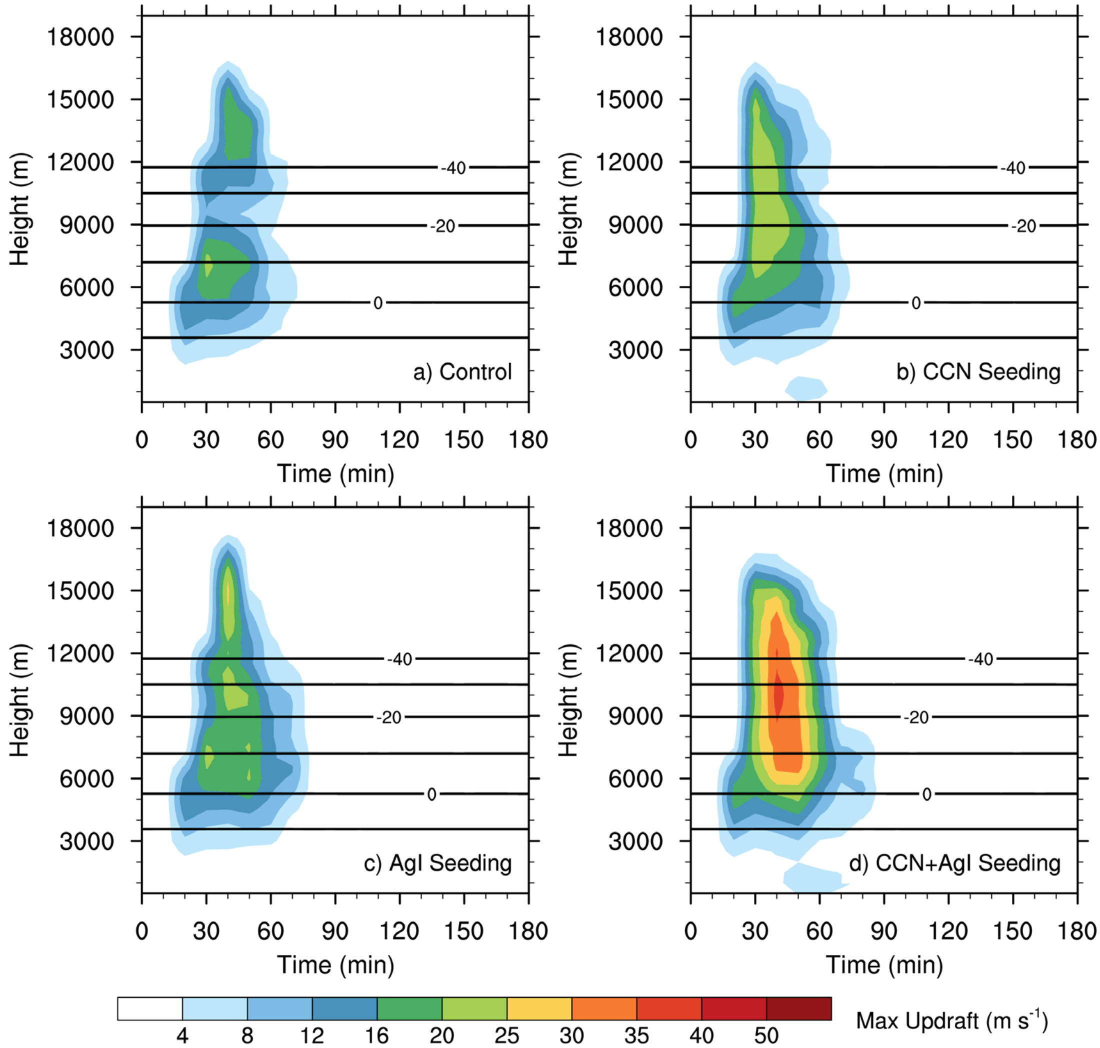

Figure 21: Time-height distribution of the domain-maximum updraft (color shaded, m s^{-1}) and temperature (black solid lines, °C) for experiments of (a) Control, (b) hygroscopic CCN seeding, (c) glaciogenic AgI seeding, and (d) the combined CCN+AgI Seeding.

Comparing to the control experiment (Fig. 22a), the individual hygroscopic CCN and glaciogenic AgI seeding significantly strengthens downdraft owning to the formation of more precipitation (Figs. 22b, c). Corresponding to the much higher mixing ratios of rainwater, snow, and graupel, the combined CCN+AgI seeding produces the strongest downdraft of −14 m s^{-1} comparing to −8 m s^{-1} in the control experiment (Fig. 22d).

https://doi.org/10.5194/egusphere-2026-5549
Preprint. Discussion started: 22 September 2026

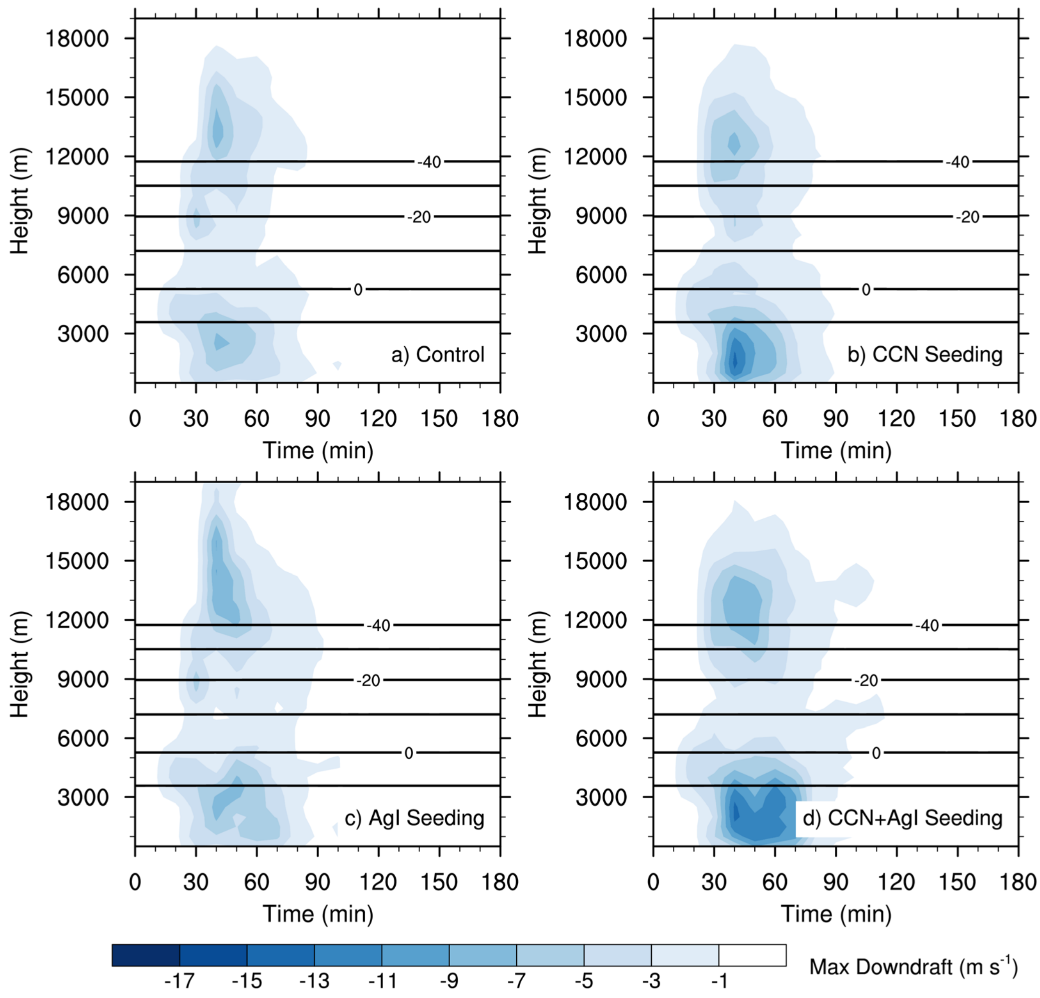

Figure 22: As in Fig. 21, but for downdraft.

4.2.3 Impacts of cloud seeding on precipitation efficiency

Precipitation efficiency (PE) is defined as the ratio of surface precipitation to the sum of net condensation and deposition (Khain et al., 2008; He et al., 2015):

$$PE = \frac{SP}{COND+SDE} \tag{12}$$

where PE is precipitation efficiency, SP is surface precipitation rate, and COND and SDE are net condensation and deposition, respectively.

PE reaches the maximum value of approximately 35% in the Control experiment (Fig. 23). In contrast, the individual hygroscopic CCN seeding slightly increases the max PE to nearly 37%, and the glaciogenic AgI seeding reduces the PE to about 31%, indicating that although both the hygroscopic and glaciogenic can increase the surface precipitation, the influential mechanisms are different. The hygroscopic seeding can enhance the conversion rate from water vapor to precipitation through artificial CCN, whereas the AgI seeding primarily glaciates the supercooled water and enhances the conversion from cloud condensates to precipitation. However, the combined seeding produces the highest PE with approximately of 39%. Since CCN seeding can increase SLW in the mixed-phase region, the subsequent AgI seeding induce the SLW to glaciate and form ice. Therefore, the combined seeding can produce higher PE and more precipitation.

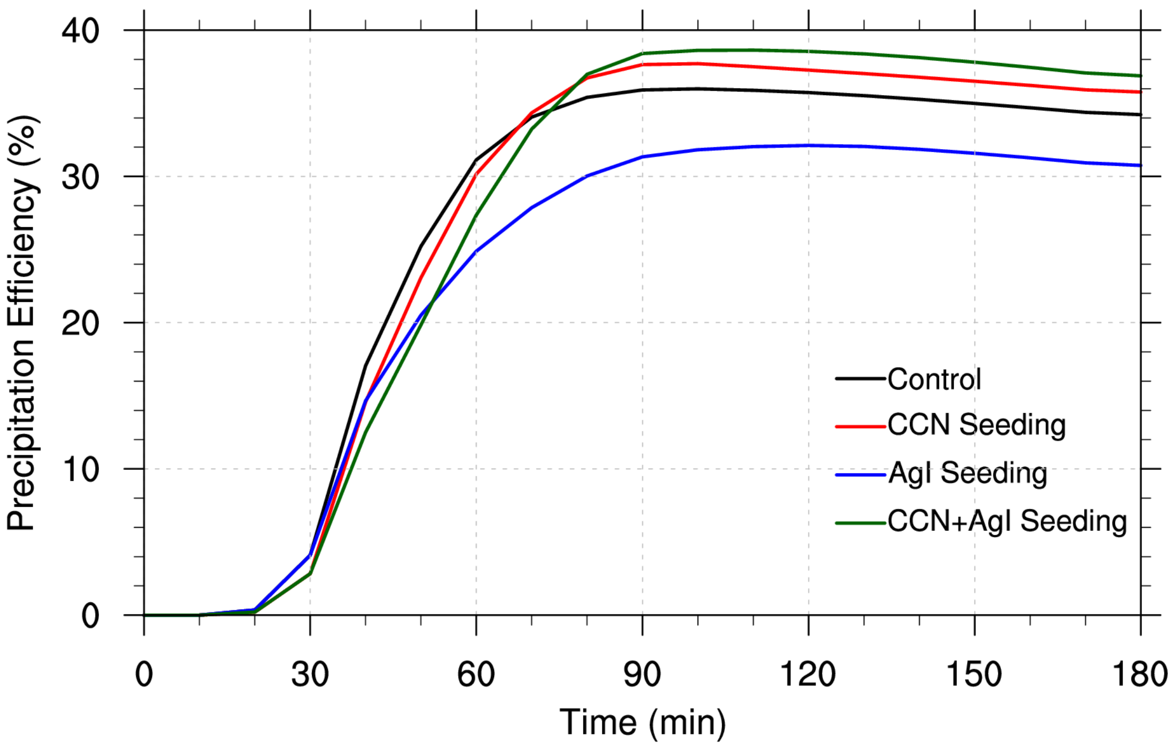

Figure 23: Temporal evolution of domain-averaged cumulative precipitation efficiency (PE, %) for experiments of Control, CCN seeding, AgI seeding, and the combined CCN+AgI seeding.

As shown above, the combined seeding is able to fully utilize the advantages of individual hygroscopic CCN seeding and glaciogenic AgI seeding, leading to much more effects on cloud microphysics, dynamics and precipitation amount. The new approach maximizes the effectiveness of artificial rain enhancement for convective clouds with a warm cloud base. The conceptual model for unseeded and seeded with the novel approach is shown in Fig. 24. The schematic illustrates the nonlinear synergistic response arising from the combined effects of CCN seeding in the warm-cloud layer and AgI seeding in the mixed-phase layer. Hygroscopic CCN is initially introduced in warm layers of approximately 2.4–4.4 km and promotes warm rain process through the enhancement of droplet activation and collision–coalescence, strengthens the updraft, and consequently enhances the upward transport of liquid water into the mixed-phase region, increasing the supply

https://doi.org/10.5194/egusphere-2026-5549
Preprint. Discussion started: 22 September 2026

of SLW. After 30 min, AgI is introduced in the mixed layers of approximately 6.6–8.6 km and promote cold rain process through the enhancement of ice nucleation, riming and the formation of snow and graupel. The cloud dynamics is also significantly strengthened in both warm and cold rain processes. Since the combined seeding greatly enhances interactions between warm and cold cloud microphysical processes, and induces much stronger dynamical response, both precipitation efficiency and surface precipitation amount are obviously increased.

https://doi.org/10.5194/egusphere-2026-5549
Preprint. Discussion started: 22 September 2026

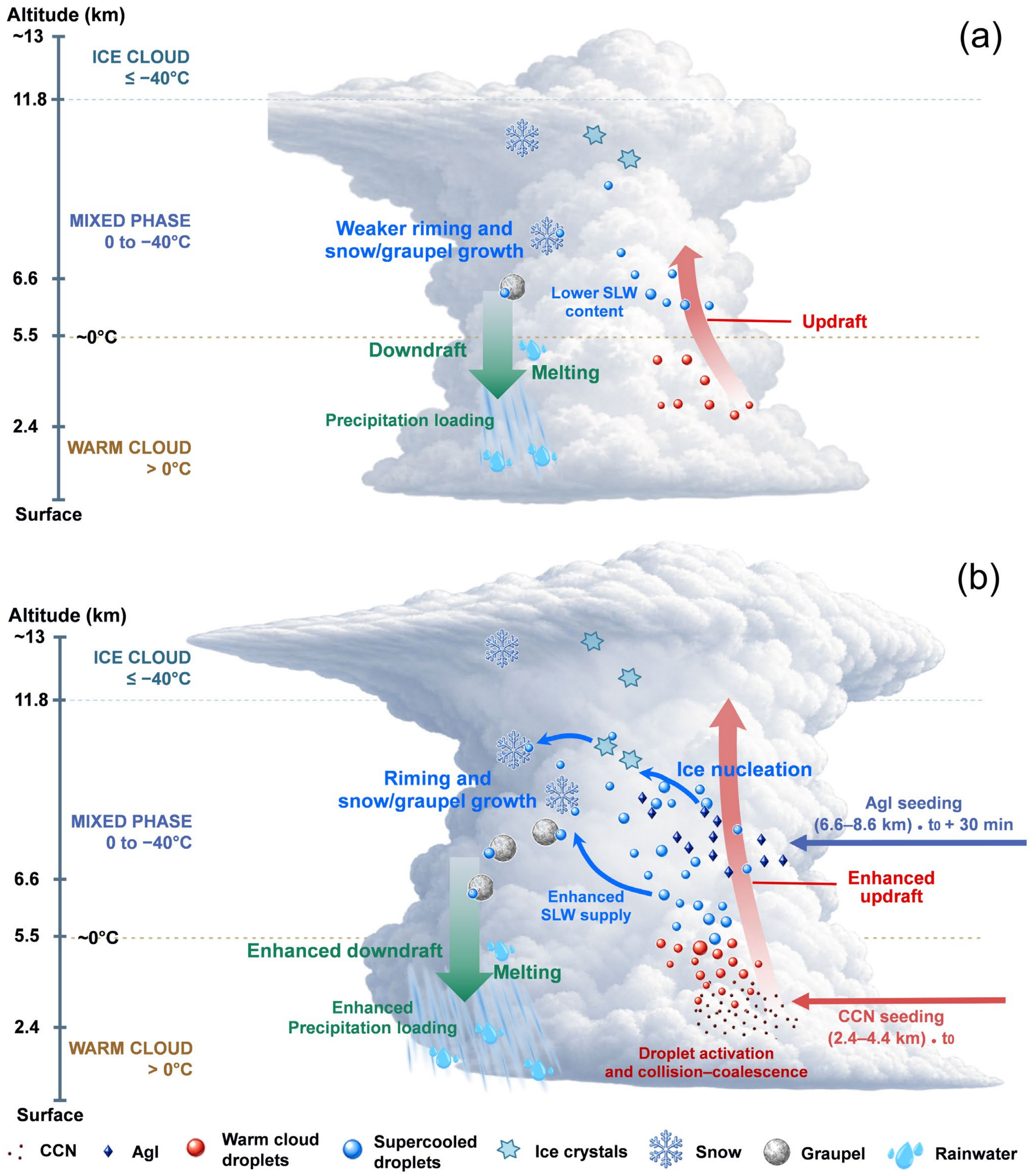

Figure 24: Conceptual model for the novel cloud seeding approach, (a) unseeded cloud, showing relatively weaker updraft, lower SLW supply, weaker riming and snow/graupel growth, and weaker precipitation loading and downdraft, and (b) the proposed novel cloud seeding through the combined hygroscopic CCN and glaciogenic AgI seeding. The initial hygroscopic CCN seeding is conducted in the warm-cloud layer (2.4–4.4 km) of the convective cloud, and then 30 min later followed by AgI seeding in the mixed-phase layer (6.6–8.6 km). The seeding strategy results in an enhanced droplet activation and then collision–coalescence, leading to stronger updraft and SLW transport, enhancing ice nucleation and riming, and subsequent snow/graupel formation, and stronger precipitation loading, melting, downdraft, and surface precipitation. Arrows illustrate the principal microphysical transport and conversion pathways associated with the coupled warm- and mixed-phase clouds and precipitation enhancement. Altitude and temperature levels are approximate for the study case.

5 Conclusions and discussion

A novel approach for efficient rain enhancement through the combined hygroscopic CCN seeding and glaciogenic AgI seeding is proposed in this study. The approach is systematically tested through WRF-based numerical simulation experiments. The associated physical mechanisms responsible for the seeding responses are examined from the aspects of cloud microphysics, dynamics and precipitation efficiency. The main conclusions are summarized as follows.

(1) For the study case, the individual glaciogenic AgI seeding and hygroscopic CCN seeding can enhance the surface precipitation of 7.97% and 20.74%, respectively, with an optimal AgI seeding rate of 0.09 g s^{-1} and CCN seeding rate of 10^{13} s^{-1}, whereas the combined hygroscopic and glaciogenic seeding approach can enhance precipitation of 57.00%. The combined seeding approach is realized through an early CCN seeding in the low warm layers, and a subsequent AgI seeding in the upper mixed-phase layers.

(2) The combined cloud seeding induces much stronger responses of cloud microphysics than individual CCN and AgI seeding. The early CCN seeding at low and warm levels can produce massive cloud droplets and enhances collision-coalescence process. Meanwhile, the cloud droplets and raindrops are transported by updraft, enhancing the formation of graupel and the supercooled LWC, which creates a more favorable condition for the AgI seeding. The subsequent AgI seeding accelerates the glaciation process and produce more snow, resulting in much more precipitation than any individual cloud seeding.

(3) The combined cloud seeding leads to stronger latent heat release and cloud dynamical response than any individual cloud seeding. The maximum updraft is only 20.5 m s^{-1} in the control (unseeded) experiment. The maximum updraft in the CCN seeding is 24.5 m s^{-1} and that in the AgI seeding is also increased but weaker than CCN seeding. The combined cloud seeding produces the strongest updraft of 36.5 m s^{-1} among all seeding experiments.

(4) The max PE reaches about 35% in control (unseeded) experiment. The CCN seeding slightly increases the max PE to 37%, and the AgI seeding reduces PE, although it enhances precipitation in this study. In contrast, the combined seeding

https://doi.org/10.5194/egusphere-2026-5549
Preprint. Discussion started: 22 September 2026

increases the max PE to be 39%, demonstrating that the proposed combined seeding approach can obviously increase PE through interactions between the seeding-induced cloud microphysics and dynamics.

The proposed combined seeding approach is established through both hygroscopic seeding and glaciogenic seeding for convective clouds with warm cloud base. The seeding approach can maximize the effectiveness of rain enhancement through interactions between the seeding-induced cloud microphysics and dynamics. The approach can be widely used in operational cloud seeding for rain enhancement of convective clouds with warm cloud base.

Previous studies have focused on the effects of individual hygroscopic/glaciogenic seeding on precipitation (Bruintjes, 1999; Guo and Zheng, 2009; Rauber et al., 2019; Li et al., 2022; Yang et al., 2024). This study proposals a novel seeding approach through combining two seeding approaches, and show that the proposed new approach can enhance the surface precipitation about 57%, which is much higher than any individual hygroscopic CCN seeding (20.74%) and glaciogenic AgI seeding (7.97%). The associated mechanisms are investigated and show that the combined cloud seeding can maximize the surface precipitation through significantly enhancing interactions between warm and cold microphysics, as well as interactions between cloud microphysics and dynamics, resulting in much higher precipitation efficiency.

However, there are some limitations for the proposed approach. The first one is that the approach is not suitable for cloud seeding on pure warm or cold convective clouds, since the precipitation formation for pure warm clouds is dominated by collision-coalescence warm rain process and that for pure cold clouds is dominated by ice processes, and the interactions between warm and cold processes are much weak in these clouds. The second one is that the simulation experiments are based on a convective precipitation case with a warm base in the southwest region in China, whether the results are suitable for other regions or not need more validations.

Data availability

The surface meteorological station data and radar observation data are available from the China National Meteorological Data Center (http://data.cma.cn/en/). ERA5 reanalysis data are available from the European Centre for Medium-Range Weather Forecasts (https://www.ecmwf.int/).

Author contributions

WS designed the experiments, performed the simulations, performed the analysis, and prepared the original manuscript. DF contributed to data analysis and interpretation and provided critical revisions to the manuscript. XG supervised the study, contributed to the interpretation of the results, and reviewed and edited the manuscript. LY contributed to data analysis and discussion of the results. XL contributed to data analysis. All authors contributed to the final version of the manuscript and approved it for publication.

https://doi.org/10.5194/egusphere-2026-5549
Preprint. Discussion started: 22 September 2026

Competing interests

The contact author has declared that none of the authors has any competing interests.

Disclaimer

Publisher's note: Copernicus Publications remains neutral with regard to jurisdictional claims in published maps and institutional affiliations.

Acknowledgements

We appreciate the anonymous reviewers for their invaluable comments that improved the quality of the manuscript.

Financial support

This research was supported by the Southwest China Artificial Weather Modification Capability Construction (Sichuan) Research and Experimental Project (SCIT-ZG(Z)-2024100001), the Second Tibetan Plateau Comprehensive Scientific Expedition (2019QZKK0104), the National Natural Science Foundation of China (42365011), and Talent Introduction Project of Chengdu University of Information Technology (KYTZ202442).

Review statement

The review statement will be added by Copernicus Publications listing the handling editor as well as all contributing referees according to their status anonymous or identified.

References

Beydoun, H., Caldwell, P. M., Stein, E. V., and Wharton, S.: Tracing the rain formation pathways in numerical simulations of deep convection, J. Adv. Model. Earth Syst., 15, e2022MS003413, https://doi.org/10.1029/2022MS003413, 2023.

Blair, D. N., Davis, B. L., and Dennis, A. S.: Cloud chamber tests of generators using acetone solutions of AgI–NaI, AgI–KI, and AgI–NH4I, J. Appl. Meteorol., 12, 1012–1017, https://doi.org/10.1175/1520-0450(1973)012<1012:CCTOGU>2.0.CO;2, 1973.

Bruintjes, R. T.: A review of cloud seeding experiments to enhance precipitation and some new prospects, Bull. Am. Meteorol. Soc., 80, 805–820, https://doi.org/10.1175/1520-0477(1999)080<0805:AROCSE>2.0.CO;2, 1999.

https://doi.org/10.5194/egusphere-2026-5549
Preprint. Discussion started: 22 September 2026

Caro, D., Wobrock, W., and Flossmann, A. I.: A numerical study on the impact of hygroscopic seeding on the development of cloud particle spectra, J. Appl. Meteorol., 41, 333–350, https://doi.org/10.1175/1520-0450(2002)041<0333:ANSOTI>2.0.CO;2, 2002.

Chen, M., Jing, X., Li, J., Yang, J., Dong, X., Geerts, B., Yin, Y., Chen, B., Xue, L., Huang, M., Tian, P., and Hua, S.: Accelerated impact of airborne glaciogenic seeding of stratiform clouds by turbulence, Atmos. Chem. Phys., 25, 7581–7596, https://doi.org/10.5194/acp-25-7581-2025, 2025.

Chen, Q., Fan, J., Hagos, S., Gustafson Jr., W. I., and Berg, L. K.: Roles of wind shear at different vertical levels: Cloud system organization and properties, J. Geophys. Res.-Atmos., 120, 6551–6574, https://doi.org/10.1002/2015JD023253, 2015.

Chen, S., Xue, L., Tessendorf, S., Chubb, T., Peace, A., Ackermann, L., Gevorgyan, A., Huang, Y., Siems, S., Rasmussen, R., Kenyon, S., and Speirs, J.: Simulating wintertime orographic cloud seeding over the Snowy Mountains of Australia, J. Appl. Meteorol. Climatol., 62, 1693–1709, https://doi.org/10.1175/JAMC-D-23-0012.1, 2023.

Cooper, W. A., Bruintjes, R. T., and Mather, G. K.: Calculations pertaining to hygroscopic seeding with flares, J. Appl. Meteorol., 36, 1449–1469, https://doi.org/10.1175/1520-0450(1997)036<1449:CPTHSW>2.0.CO;2, 1997.

DeMott, P. J.: Quantitative descriptions of ice formation mechanisms of silver iodide-type aerosols, Atmos. Res., 38, 63–99, https://doi.org/10.1016/0169-8095(94)00088-U, 1995.

Dong, X., Chen, B., Yang, J., and Mai, R.: Response of cloud microphysics to aircraft-based glaciogenic seeding of supercooled clouds in North China, Atmos. Res., 329, 108502, https://doi.org/10.1016/j.atmosres.2025.108502, 2026.

Fang, C. G., Guo, X. L., and Wang, P. X.: The physical and precipitation response to AgI-seeding from a mesoscale WRF-based seeding model [in Chinese], Chinese J. Atmos. Sci., 33, 621–633, https://doi.org/10.3878/j.issn.1006-9895.2009.03.18, 2009.

Fankhauser, J. C.: Estimates of thunderstorm precipitation efficiency from field measurements in CCOPE, Mon. Weather Rev., 116, 663–684, https://doi.org/10.1175/1520-0493(1988)116<0663:EOTPEF>2.0.CO;2, 1988.

Feingold, G. and Heymsfield, A. J.: Parameterizations of condensational growth of droplets for use in general circulation models, J. Atmos. Sci., 49, 2325–2342, https://doi.org/10.1175/1520-0469(1992)049<2325:POCGOD>2.0.CO;2, 1992.

Flossmann, A. I., Manton, M., Abshaev, A., Bruintjes, R., Murakami, M., Prabhakaran, T., and Yao, Z.: Review of advances in precipitation enhancement research, Bull. Am. Meteorol. Soc., 100, 1465–1480, https://doi.org/10.1175/BAMS-D-18-0160.1, 2019.

Fonseca, R., Francis, D., Nelli, N., Farrah, S., Wehbe, Y., Al Hosari, T., and Al Mazroui, A.: Assessment of the WRF model as a guidance tool into cloud seeding operations in the United Arab Emirates, Earth Space Sci., 9, e2022EA002269, https://doi.org/10.1029/2022EA002269, 2022.

French, J. R., Friedrich, K., Tessendorf, S. A., Rauber, R. M., Geerts, B., Rasmussen, R. M., Xue, L., Kunkel, M. L., and Blestrud, D. R.: Precipitation formation from orographic cloud seeding, Proc. Natl. Acad. Sci., 115, 1168–1173, https://doi.org/10.1073/pnas.1716995115, 2018.

https://doi.org/10.5194/egusphere-2026-5549
Preprint. Discussion started: 22 September 2026

Freud, E., Koussevitzky, H., Goren, T., and Rosenfeld, D.: Cloud microphysical background for the Israel-4 cloud seeding experiment, Atmos. Res., 158, 122–138, https://doi.org/10.1016/j.atmosres.2015.02.007, 2015.

Gao, S. and Li, X.: The dependence of precipitation efficiency on rainfall type in a cloud-resolving model, J. Geophys. Res.-Atmos., 116, D21207, https://doi.org/10.1029/2011JD016117, 2011.

Garstang, M., Bruintjes, R., Serafin, R., Orville, H., Boe, B., Cotton, W., and Warburton, J.: Weather modification: Finding common ground, Bull. Am. Meteorol. Soc., 86, 647–655, https://doi.org/10.1175/BAMS-86-5-647, 2005.

Geerts, B. and Rauber, R. M.: Glaciogenic seeding of cold-season orographic clouds to enhance precipitation: Status and prospects, Bull. Am. Meteorol. Soc., 103, E2302–E2314, https://doi.org/10.1175/BAMS-D-21-0279.1, 2022.

Guo, X. L. and Zheng, G. G.: Advances in weather modification from 1997 to 2007 in China, Adv. Atmos. Sci., 26, 240–252, https://doi.org/10.1007/s00376-009-0240-8, 2009.

Guo, X. L., Zheng, G. G., and Jin, D. Z.: A numerical comparison study of cloud seeding by silver iodide and liquid carbon dioxide, Atmos. Res., 79, 183–226, https://doi.org/10.1016/j.atmosres.2005.04.005, 2006.

Guo, X. L., Fu, D. H., and Zheng, G. G.: Modeling study on optimal convective cloud seeding in rain augmentation, J. Korean Meteor. Soc., 43, 273–284, available at: https://www.kci.go.kr/kciportal/ci/sereArticleSearch/ciSereArtiView.kci?sereArticleSearchBean.artiId=ART001076301, 2007.

Guo, X. L., Fu, D. H., Li, X. Y., Hu, Z. X., Lei, H. C., Xiao, H., and Hong, Y. C.: Advances in cloud physics and weather modification in China, Adv. Atmos. Sci., 32, 230–249, https://doi.org/10.1007/s00376-014-0006-9, 2015.

He, H., Liu, X., Xue, L., and Gao, Q.: Mesoscale numerical simulation on the precipitation enhancement of stratiform clouds with embedded convection, Atmos. Res., 286, 106672, https://doi.org/10.1016/j.atmosres.2023.106672, 2023.

Hoffmann, F. and Feingold, G.: Cloud microphysical implications for marine cloud brightening: The importance of the seeded particle size distribution, J. Atmos. Sci., 78, 3247–3262, https://doi.org/10.1175/JAS-D-21-0077.1, 2021.

Huang, Y. J. and Cui, X. P.: Dominant cloud microphysical processes of a torrential rainfall event in Sichuan, China, Adv. Atmos. Sci., 32, 389–400, https://doi.org/10.1007/s00376-014-4066-7, 2015.

Jensen, J. B. and Lee, S.: Giant sea-salt aerosols and warm rain formation in marine stratocumulus, J. Atmos. Sci., 65, 3678–3694, https://doi.org/10.1175/2008JAS2617.1, 2008.

Köhler, H.: The nucleus in and the growth of hygroscopic droplets, Trans. Faraday Soc., 32, 1152–1161, https://doi.org/10.1039/TF9363201152, 1936.

Koop, T., Luo, B., Tsias, A., and Peter, T.: Water activity as the determinant for homogeneous ice nucleation in aqueous solutions, Nature, 406, 611–614, https://doi.org/10.1038/35020537, 2000.

Kuba, N. and Murakami, M.: Effect of hygroscopic seeding on warm rain clouds – numerical study using a hybrid cloud microphysical model, Atmos. Chem. Phys., 10, 3335–3351, https://doi.org/10.5194/acp-10-3335-2010, 2010.

https://doi.org/10.5194/egusphere-2026-5549
Preprint. Discussion started: 22 September 2026

Li, D., Zhao, C., Li, P., Liu, C., Gong, D., Liu, S., Yuan, Z., and Chen, Y.: Macro- and micro-physical characteristics of different parts of mixed convective-stratiform clouds and differences in their responses to seeding, Adv. Atmos. Sci., 39, 2040–2055, https://doi.org/10.1007/s00376-022-2003-8, 2022.

Lin, K.-I., Chung, K.-S., Wang, S.-H., Chen, L.-H., Liou, Y.-C., Lin, P.-L., Chang, W.-Y., Chiu, H.-J., and Chang, Y.-H.: Evaluation of hygroscopic cloud seeding in warm-rain processes by a hybrid microphysics scheme using a Weather Research and Forecasting (WRF) model: A real case study, Atmos. Chem. Phys., 23, 10423–10438, https://doi.org/10.5194/acp-23-10423-2023, 2023.

Lou, X. F., Shi, Y. Q., Sun, J., Xue, L. L., Hu, Z. J., Fang, W., and Liu, W. G.: Cloud-resolving model for weather modification in China, Chinese Sci. Bull., 57, 1055–1061, https://doi.org/10.1007/s11434-011-4934-9, 2012.

Mazzetti, T., Geerts, B., and Xue, L.: A numerical evaluation of the impact of operational ground-based glaciogenic cloud seeding on precipitation over the Wind River Range, Wyoming, J. Appl. Meteorol. Climatol., 62, 489–510, https://doi.org/10.1175/JAMC-D-22-0132.1, 2023.

Meyers, M. P., DeMott, P. J., and Cotton, W. R.: A comparison of seeded and nonseeded orographic cloud simulations with an explicit cloud model, J. Appl. Meteorol., 34, 834–846, https://doi.org/10.1175/1520-0450(1995)034<0834:ACOSAN>2.0.CO;2, 1995.

National Research Council: Critical issues in weather modification research, The National Academies Press, Washington, DC, https://doi.org/10.17226/10829, 2003.

Orville, H. D.: A review of cloud modeling in weather modification, Bull. Am. Meteorol. Soc., 77, 1535–1555, https://doi.org/10.1175/1520-0477(1996)077<1535:AROCMI>2.0.CO;2, 1996.

Orville, H. D. and Chen, J. M.: Effects of cloud seeding, latent heat of fusion, and condensate loading on cloud dynamics and precipitation evolution: A numerical study, J. Atmos. Sci., 39, 2807–2827, https://doi.org/10.1175/1520-0469(1982)039<2807:EOCSLH>2.0.CO;2, 1982.

Pokharel, B., Geerts, B., and Jing, X.: The impact of ground-based glaciogenic seeding on orographic clouds and precipitation: A multisensor case study, J. Appl. Meteorol. Clim., 53, 890–909, https://doi.org/10.1175/JAMC-D-13-0290.1, 2014.

Prabhakaran, T., Murugavel, P., Konwar, M., Malap, N., Gayatri, K., Dixit, S., Samanta, S., Chowdhuri, S., Bera, S., Varghese, M., Rao, J., Sandeep, J., Safai, P. D., Sahai, A. K., Axisa, D., Karipot, A., Baumgardner, D., Werden, B., Fortner, E., Hibert, K., Nair, S., Bankar, S., Gurnule, D., Todekar, K., Jose, J., Jayachandran, V., Soyam, P. S., Gupta, A., Choudhary, H., Aravindhavel, A., Kantipudi, S. B., Pradeepkumar, P., Krishnan, R., Nandakumar, K., DeCarlo, P. F., Worsnop, D., Bhat, G. S., Rajeevan, M., and Nanjundiah, R.: CAIPEEX: Indian cloud seeding scientific experiment, Bull. Am. Meteorol. Soc., 104, E2095–E2120, https://doi.org/10.1175/BAMS-D-21-0291.1, 2023.

Qi, D., Li, Y., Zhou, C., and Chen, D.: Climatic change of summer rainstorms and the water vapor budget in the Sichuan Basin, J. Appl. Meteorol. Clim., 61, 537–557, https://doi.org/10.1175/JAMC-D-21-0100.1, 2022.

https://doi.org/10.5194/egusphere-2026-5549
Preprint. Discussion started: 22 September 2026

Qian, T., Zhao, P., Zhang, F., and Bao, X.: Rainy-season precipitation over the Sichuan Basin and adjacent regions in southwestern China, Mon. Weather Rev., 143, 383–394, https://doi.org/10.1175/MWR-D-13-00158.1, 2015.

Rauber, R. M., Geerts, B., Xue, L., French, J., Friedrich, K., Rasmussen, R. M., Tessendorf, S. A., Blestrud, D. R., Kunkel, M. L., and Parkinson, S.: Wintertime orographic cloud seeding—A review, J. Appl. Meteorol. Climatol., 58, 2117–2140, https://doi.org/10.1175/JAMC-D-18-0341.1, 2019.

Reisin, T., Tzivion, S., and Levin, Z.: Seeding convective clouds with ice nuclei or hygroscopic particles: A numerical study using a model with detailed microphysics, J. Appl. Meteorol., 35, 1416–1434, https://doi.org/10.1175/1520-0450(1996)035<1416:SCCWIN>2.0.CO;2, 1996.

Rosenfeld, D., Axisa, D., and Woodley, W. L.: A quest for effective hygroscopic cloud seeding, J. Appl. Meteorol. Climatol., 49, 1548–1562, https://doi.org/10.1175/2010JAMC2307.1, 2010.

Segal, Y., Khain, A., Pinsky, M., and Rosenfeld, D.: Effects of hygroscopic seeding on raindrop formation as seen from simulations using a 2000-bin spectral cloud parcel model, Atmos. Res., 71, 3–34, https://doi.org/10.1016/j.atmosres.2004.03.003, 2004.

Shu, W. X., Xiao, H., Fu, D. H., Yang, H. L., Shen, S. J., and Sun, Y.: Effects of cloud condensation nuclei concentration on the evolution of severe convective storms, Atmos. Res., 276, 106252, https://doi.org/10.1016/j.atmosres.2022.106252, 2022.

Silverman, B. A.: A critical assessment of hygroscopic seeding of convective clouds for rainfall enhancement, Bull. Am. Meteorol. Soc., 84, 1219–1230, https://doi.org/10.1175/BAMS-84-9-1219, 2003.

Skamarock, W. C., Klemp, J. B., Dudhia, J., Gill, D. O., Liu, Z., Berner, J., Wang, W., Powers, J. G., Duda, M. G., Barker, D. M., and Huang, X. Y.: A description of the Advanced Research WRF Version 4, NCAR Tech. Note NCAR/TN-556+STR, 145 pp., https://doi.org/10.5065/1dfh-6p97, 2019.

Sun, J., Shi, Z., Chai, J., Xu, G., and Niu, B.: Effects of mixed phase microphysical process on precipitation in a simulated convective cloud, Atmosphere, 7, 97, https://doi.org/10.3390/atmos7080097, 2016.

Tessendorf, S. A., Chen, S., Weeks, C., Bruintjes, R., Rasmussen, R. M., and Xue, L.: The influence of hygroscopic flare seeding on drop size distribution over Southeast Queensland, J. Geophys. Res.-Atmos., 126, e2020JD033771, https://doi.org/10.1029/2020JD033771, 2021.

Thompson, G., Field, P. R., Rasmussen, R. M., and Hall, W. D.: Explicit forecasts of winter precipitation using an improved bulk microphysics scheme. Part II: Implementation of a new snow parameterization, Mon. Weather Rev., 136, 5095–5115, https://doi.org/10.1175/2008MWR2387.1, 2008.

Thompson, G., and Eidhammer, T.: A study of aerosol impacts on clouds and precipitation development in a large winter cyclone, J. Atmos. Sci., 71, 3636–3658, https://doi.org/10.1175/JAS-D-13-0305.1, 2014.

Tonttila, J., Afzalifar, A., Kokkola, H., Raatikainen, T., Korhonen, H., and Romakkaniemi, S.: Precipitation enhancement in stratocumulus clouds through airborne seeding: Sensitivity analysis by UCLALES-SALSA, Atmos. Chem. Phys., 21, 1035–1048, https://doi.org/10.5194/acp-21-1035-2021, 2021.

https://doi.org/10.5194/egusphere-2026-5549
Preprint. Discussion started: 22 September 2026

Tonttila, J., Korpinen, A., Kokkola, H., Romakkaniemi, S., Fortelius, C., and Korhonen, H.: Interaction between hygroscopic seeding and mixed-phase microphysics in convective clouds, J. Appl. Meteorol. Climatol., 61, 1533–1547, https://doi.org/10.1175/JAMC-D-21-0183.1, 2022.

Wang, W., Liu, J., Shi, L., Liu, P., Zhang, S., and Dong, X.: Case analysis of microphysical characteristics of precipitation cloud system in Sichuan Basin [in Chinese], Meteorological Monthly, 37, 1389–1394, https://doi.org/10.7519/j.issn.1000-0526.2011.11.009, 2011.

Wang, F., Li, Z., Jiang, Q., Wang, G., Jia, S., Duan, J., and Zhou, Y.: Evaluation of hygroscopic cloud seeding in liquid-water clouds: A feasibility study, Atmos. Chem. Phys., 19, 14967–14977, https://doi.org/10.5194/acp-19-14967-2019, 2019.

Wang, J., Yue, Z., Rosenfeld, D., Zhang, L., Zhu, Y., Dai, J., Yu, X., and Li, J.: The evolution of an AgI cloud-seeding track in central China as seen by a combination of radar, satellite, and disdrometer observations, J. Geophys. Res.-Atmos., 126, e2020JD033914, https://doi.org/10.1029/2020JD033914, 2021.

Wang, X., Zhang, L., and Moran, M. D.: Uncertainty assessment of current size-resolved parameterizations for below-cloud particle scavenging by rain, Atmos. Chem. Phys., 10, 5685–5705, https://doi.org/10.5194/acp-10-5685-2010, 2010.

Wei, L., Shi, Y., Liu, W., Li, G., Hu, W., Cai, M., Lei, H., Zhao, S., and Fu, Y.: Snow-enhancement conditions and seeding simulation of stratiform clouds in the Bayanbulak test area in China, J. Meteorol. Res., 38, 1078–1092, https://doi.org/10.1007/s13351-024-4003-3, 2024.

Weston, M. J., Temimi, M., Burger, R. P., Piketh, S. J., and Formenti, P.: Sensitivity analysis of an aerosol-aware microphysics scheme in Weather Research and Forecasting (WRF) during case studies of fog in Namibia, Atmos. Chem. Phys., 22, 10221–10245, https://doi.org/10.5194/acp-22-10221-2022, 2022.

Xia, R., Luo, Y., Zhang, D. L., Li, M., Bao, X., and Sun, J.: On the diurnal cycle of heavy rainfall over the Sichuan Basin during 10–18 August 2020, Adv. Atmos. Sci., 38, 2183–2200, https://doi.org/10.1007/s00376-021-1118-7, 2021.

Xue, L. L., Hashimoto, A., Murakami, M., Rasmussen, R., Tessendorf, S. A., Breed, D., Parkinson, S., Holbrook, P., and Blestrud, D.: Implementation of a silver iodide cloud-seeding parameterization in WRF. Part I: Model description and idealized 2D sensitivity tests, J. Appl. Meteorol. Climatol., 52, 1433–1457, https://doi.org/10.1175/JAMC-D-12-0148.1, 2013a.

Xue, L. L., Tessendorf, S. A., Nelson, E., Rasmussen, R., Breed, D., Parkinson, S., Holbrook, P., and Blestrud, D.: Implementation of a silver iodide cloud-seeding parameterization in WRF. Part II: 3D simulations of actual seeding events and sensitivity tests, J. Appl. Meteorol. Climatol., 52, 1458–1476, https://doi.org/10.1175/JAMC-D-12-0149.1, 2013b.

Yang, J., Li, J., Chen, M., Jing, X., Yin, Y., Geerts, B., Wang, Z., Liu, Y., Chen, B., Hua, S., Hu, H., Dong, X., Tian, P., Chen, Q., and Gao, Y.: Estimating the concentration of silver iodide needed to detect unambiguous signatures of glaciogenic cloud seeding, Atmos. Chem. Phys., 24, 13833–13848, https://doi.org/10.5194/acp-24-13833-2024, 2024.

Yin, Y., Levin, Z., Reisin, T., and Tzivion, S.: Seeding convective clouds with hygroscopic flares: Numerical simulations using a cloud model with detailed microphysics, J. Appl. Meteorol., 39, 1460–1472, https://doi.org/10.1175/1520-0450(2000)039<1460:SCCWHF>2.0.CO;2, 2000.